Electrodeposition-Assisted Synthesis of Fe-doped NiCo Layered Double Hydroxide Nanosheets for Efficient Oxygen Evolution Reaction

Cheru Fekadu Molla

A Thesis Submitted to the Department of Applied Chemistry

School of Applied Natural Science

Presented in Partial Fulfillment of the Requirement for the Degree of Master's in Applied Chemistry (Physical Chemistry)

Office of Graduate Studies

Adama Science and Technology University

June, 2022

Adama, Ethiopia

Electrodeposition-Assisted Synthesis of Fe-doped NiCo Layered Double Hydroxide Nanosheets for Efficient Oxygen Evolution Reaction

Cheru Fekadu Molla

Major Advisor: Lemma Teshome Tufa (Ph.D.)

Co-Advisors: Bedassa Abdissa Gonfa (Ph.D.)

Fedlu Kedir Sabir (Ph.D.)

A Thesis Submitted to the Department of Applied Chemistry
School of Applied Natural Science

Presented in Partial Fulfillment of the Requirement for the Degree of Master's in Applied Chemistry (Physical Chemistry)

Office of Graduate Studies

Adama Science and Technology University

June, 2022

Adama, Ethiopia

Declaration

I hereby declare that this Master Thesis entitled **"Electrodeposition-Assisted Synthesis of Fe-doped NiCo Layered Double Hydroxide Nanosheets for Efficient Oxygen Evolution Reaction**" is my original work. That is, it has not been submitted for the award of any academic degree, diploma, or certificate in any other university. All sources of materials that are used for this thesis have been duly acknowledged through citation.

_____ _____ _____

Name of student Signature Date

Recommendation of Advisors

We, the advisors of this thesis, hereby certify that we have read the revised version of the thesis entitled "**Electrodeposition-Assisted Synthesis of Fe-doped NiCo Layered Double Hydroxide Nanosheets for Efficient Oxygen Evolution Reaction**" prepared under our guidance by **Cheru Fekadu** submitted in partial fulfillment of the requirements for the degree of Masters of Science in Applied Chemistry (Physical Chemistry). Therefore, we recommend the submission of a revised version of the thesis to the department following the applicable procedures.

Lemma Teshome Tufa (Ph.D.)		06/06/2022
Major Advisor	Signature	Date
_____	_____	_____
Co-Advisor	Signature	Date
_____	_____	_____
Co-Advisor	Signature	Date

Thesis Approval Sheet

We, the advisors of the thesis entitled "**Electrodeposition-Assisted Synthesis of Fe-doped NiCo Layered Double Hydroxide Nanosheets for Efficient Oxygen Evolution Reaction**" and developed by **Cheru Fekadu**, hereby certify that the recommendation and suggestions made by the board of examiners are appropriately incorporated into the final version of the thesis.

Lemma Teshome Tufa (Ph.D.)		06/06/2022
Major Advisor	Signature	Date
_____	_____	_____
Co-Advisor	Signature	Date
_____	_____	_____
Co-Advisor	Signature	Date

Approval of Board of Reviewers

We, the undersigned, members of the Board of Examiners of the thesis by **Cheru Fekadu** have read and evaluated the thesis entitled "**Electrodeposition-Assisted Synthesis of Fe-doped NiCo Layered Double Hydroxide Nanosheets for Efficient Oxygen Evolution Reaction**" and examined the candidate during open defense. This is, therefore, to certify that the thesis is accepted for partial fulfillment of the requirement of the degree of Master of Science in Applied Chemistry (Physical Chemistry).

_____	_____	_____
Chairperson	Signature	Date
_____	_____	_____
Internal Examiner	Signature	Date
_____	_____	_____
External Examiner	Signature	Date

Final approval and acceptance of the thesis is contingent upon submission of its final copy to the Office of Postgraduate Studies (OPGS) through the Department Graduate Council (DGC) and School Graduate Committee (SGC).

_____	_____	_____
Department Head	Signature	Date
_____	_____	_____
School Dean	Signature	Date
_____	_____	_____
Office of Postgraduate Studies, Dean	Signature	Date

Acknowledgments

First and foremost, I would like to thank Almighty God for giving me the strength, knowledge, and ability and his mother St. Mary for their invaluable help in allowing me to accomplish my M.Sc. program successfully.

Next, I would like to express my sincere gratitude to my advisor, Lemma Teshome (Ph.D.), for his professional, technical, very invaluable, and unreserved advice, guidance, and constructive criticism support during the whole period of this thesis work.

I would like to express my deepest gratitude to my Co-Advisors, Fedlu Kedir (Ph.D.) and Bedassa Abdissa (Ph.D.) for their patience, fruitful advice, and friendly approach throughout my work.

Furthermore, I would like to give the dearest and greatest thanks to Mr. Endale Kebede from the School of Applied Natural Science, Department of Applied Chemistry program for his willingness to share his knowledge and experience about methods of synthesis of the nanosheets.

Last but not least, I would like to express my sincere gratitude to all academic, technical, and support staff of the Program of Applied Chemistry, Adama Science and Technology University for providing the necessary knowledge, assistance, and facilities to conduct my research work.

Table of Content

Acknowledgments i

List of Acronyms and Abbreviations iii

List of Figures iv

List of Tables v

Abstract vi

1. INTRODUCTION 1

1.1. Background of the Study 1

1.2. Statement of the Problem 3

1.3. Objectives of the Study 4

1.3.1. General Objective 4

1.3.2. Specific Objectives 4

1.4. Significance of the Study 4

1.5. Scope of the Study 5

2. LITERATURE REVIEW 6

2.1. Electrocatalytic Water Splitting 6

2.1.1. Oxygen Evolution Reaction (OER) 7

2.1.2. Evaluation Parameters for OER 10

2.2. Ni-based LDH NSs 12

2.3. Effect of Fe-doping in Ni-based LDH NSs 14

2.4. Typical Synthetic and Fabrication Methods of Ni-based LDH NSs 16

2.4.1. Hydro/Solvothermal Synthesis Method 16

2.4.2. Co-precipitation Method 18

2.4.3. Electrochemical Deposition Method 20

2.4.4. Other Methods 22

3. MATERIALS AND METHODS 24
3.1. Study Site Description 24
3.2. Chemicals and Reagents 24
3.3. Synthesis of Fe-NiCo LDH NSs Electrocatalysts 24
3.4. Characterization of Fe-NiCo LDH NSs 25
3.5. Electrochemical Measurements 25
4. RESULTS AND DISCUSSION 27
4.1. Fabrication and Characterization of Fe-NiCo LDH NSs 27
4.2. OER Catalytic Performance 33
5. CONCLUSIONS AND RECOMMENDATIONS 44
5.1. Conclusions 44
5.2. Recommendations 44
6. REFERENCES 45
Appendix 57
I. List of Publications/Manuscript in Preparation 57
II. Supporting Information 58

List of Acronyms and Abbreviations

2D	Two-dimensional
3D	Three-dimensional
AFM	Atomic Force Microscopy
C_{dl}	Double-layer Capacitances
CE	Counter Electrode
CFC	Carbon Fiber Cloth
CVs	Cyclic Voltammograms
DFT	Density Functional Theory
ECSA	Electrochemically Active Surface Area
EDS	Energy-Dispersive X-Ray Spectroscopy
EIS	Electrochemical Impedance Spectroscopy
FTO	Fluorine doped Tin Oxide
HER	Hydrogen Evolution Reaction
LDHs	Layered Double Hydroxides
LSVs	Linear Sweep Voltammograms
NF	Nickel Foam
NSs	Nanosheets
OECs	Oxygen Evolving Catalysts
OER	Oxygen Evolution Reaction
RHE	Reversible Hydrogen Electrode
SCE	Saturated Calomel Electrode
SEM	Scanning Electron Microscope
TEM	Transmission Electron Microscopy
TMOs	Transition Metal Oxides
TMPs	Transition Metal Phosphines
V_{op}	Overall Operational Voltage
XPS	X-ray Photoelectron Spectroscopy
XRD	X-ray Diffraction

List of Figures

Figure 1: a) OER mechanisms in acid (blue) and alkaline (red) conditions. (b) Typical structure model of LDHs and in-plane cation arrangement. Copyright (2020), Springer. 10
Figure 2: (a) XRD spectrum of bare FTO, NiCo LDH, and Fe-NiCo LDH material, (b) HRTEM of Fe-NiCo LDH. 28
Figure 3: (a) SEM and (b) TEM image of Fe-NiCo LDH. 29
Figure 4: (a) SEM-EDS image, (b) The corresponding elemental mapping of Fe-NiCo LDH... 30
Figure 5: SEM-EDS spectrum of Fe-NiCo LDH. 30
Figure 6: XPS survey plots of (a) Fe-doped NiCo LDH/NF and (b) Undoped NiCo LDH/NF.. 32
Figure 7: High-resolution XPS spectra of the Fe-NiCo LDH/NF: (a) Ni 2p, (b) Co 2p, (c) Fe 2p and (d) O 1s. 33
Figure 8: Electrochemical characteristics of the electrodes upon immersion in 1 M KOH aqueous solution. (a) CV curves recorded at a scan rate of 5 mV s^{-1}. (b) CV curves of NiCo-4Fe LDH at various scan rates. 34
Figure 9: Electrochemical performance of various Fe-NiCo-LDH/NF electrodes carried out under a constant current density of 10 mA cm^{-2} in 1 M KOH aqueous solution. (a) OER polarization curves, (b) Overpotential comparison. 35
Figure 10: Tafel curve of various Fe-NiCo-LDH carried out under a constant current density of 10 mA cm^{-2}. 36
Figure 11: Double layer capacitance measurements with scan rates at 2, 4, 6, 8, and 10 mV/s in the region of 0.3–0.4 V vs. RHE for Fe NiCo LDH/NF. 38
Figure 12: Capacitive current differences ($\Delta j = j_{anode} — j_{cathode}$) at 0.35 V vs RHE against scan rates of Fe-NiCo-LDH carried out under a constant current density of 10 mA cm^{-2}. 39
Figure 13: Nyquist plots of Fe-NiCo LDH carried out under a constant current density of 10 mA cm^{-2} and equivalent electrical circuit inset. 42
Figure 14: (a) Long-term stability test carried out under a constant current density of 10 mA cm^{-2}, (b) Multistep chronopotentiometric curve for Fe-NiCo LDH. 43

List of Tables

Table 1: Evaluation parameters for OER and their applications..... 11

Table 2: Elemental composition of Fe-NiCo LDH NSs sample from EDS analysis..... 31

Table 3: Comparison of the electrocatalytic activity of the as-prepared Fe-NiCo LDH (current density of 10 mA cm^{-2}) NSs toward OER with previously reported LDH-based catalysts..... 36

Table 4: ECSA results estimated from C_{dl} for the as-fabricated samples for OER. 40

Abstract

Hydrogen, as a sustainable and green energy carrier, is an ideal alternative to traditional fossil fuels to solve the aggravating energy crisis and environmental pollution. However, industrial production of hydrogen from water splitting is mainly hindered by sluggish kinetics of oxygen evolution reactions (OER) at the anode in alkaline solution due to the difficulty in forming binding protons. Thus, the development of robust, highly active, and cost-efficient catalyst is critical to enhance reaction efficiency and decreasing required overpotential. Layered double hydroxides (LDHs) containing first-row transition metals (e.g., iron (Fe), cobalt (Co), and nickel (Ni)) have attracted significant interest for electrocatalytic applications owing to their earth abundance and excellent performance for OER in alkaline media. Herein, Fe-doped NiCo LDH (Fe-NiCo LDH) nanosheets (NSs) with a hierarchical nanostructure were successfully fabricated on nickel foam (NF) via a facile electrochemical deposition method. The optimum Fe-NiCo-LDH NS sample shows a low overpotential of 189 mV at a current density of 10 mA cm^{-2} and a low Tafel slope of 98.7 mV dec^{-1}. The enhanced OER activity of the Fe-NiCo LDH catalyst is attributed to (i) the high specific surface area of the nanosheets, which is beneficial for increasing the number of active sites and (ii) the improved kinetics and enhanced ion transport arising from iron doping and synergistic effects. This study provides an effective avenue to fabricate efficient cation-doped multimetallic LDH electrocatalysts for efficient water splitting.

Key words: *Ultrathin Nanosheets, Electrochemical Deposition, Oxygen Evolution Reactions, Fe-doping, Catalytic Activity, and NiCo LDH.*

1. INTRODUCTION

1.1. Background of the Study

An increase in global demand for energy coupled with the rising environmental concerns related to fossil fuel use has motivated the world to search for alternative energy sources that are efficient, affordable, and environment friendly (Friebel et al., 2015; Gicha, Tufa, Kang, et al., 2021). Among various approaches, electrocatalytic water splitting powered by renewable energy sources has been recognized as a promising technology for large-scale hydrogen production with zero carbon footprint (Guo et al., 2020). To ensure high efficiency of water splitting, electrocatalysts are indispensable to accelerate sluggish kinetics and reduce overpotentials required to produce hydrogen (Gicha, Tufa, Kang, et al., 2021; Guo et al., 2020). Assistance of electrocatalyst is needed to increase efficiency and lower large water splitting energy (i.e., thermodynamically uphill reaction for water splitting process requires Gibbs free energy of (ΔG) $\approx$ 237.2 KJ mol^{-1}, corresponding to a standard potential (ΔE) of 1.23 V *versus* reversible hydrogen electrode (RHE) (Hunter, Gray, & Muller, 2016).

The imminent shortage of traditional fossil fuels has prompted researchers to develop highly efficient renewable energy conversion and storage systems, such as rechargeable batteries, solar cells, and water splitting. The process of electrochemical water splitting involves two main half-reactions: Oxygen evolution reaction (OER) at the anodic side and hydrogen evolution reaction (HER) at the cathodic side. Still, the large scale production of hydrogen *via* water splitting technology is currently limited by the slow kinetics of the anodic OER which involves a four-step proton-coupled electron transfer (A.-L. Wang, Xu, & Li, 2016). Hence, the development of electrocatalysts with enhanced kinetics for OER is crucial for accelerating the process of water splitting. At present, noble metal based materials, such as Ir- or Ru-based oxides are generally served as the benchmark owing to their excellent catalytic performance for OER (Wu, Zou, Huang, & Gao, 2018). However, the scarcities, expensive and low stability of these noble-metal-based electrocatalysts hinder their widespread application. To address these challenges, numerous research efforts have been conducted to develop low-cost and high-performance non-precious electrocatalysts based on transition metal oxides (TMOs), (Bhanja et al., 2019)

hydroxides, (Septiani et al., 2020; Wu, Wang, Huang, & Gao, 2018; Zhou et al., 2017) sulfides, (L. Li et al., 2019) phosphides, (Septiani et al., 2020) and selenides (C. Cai et al., 2019).

Among them, Layered double hydroxides (LDHs) have gained increasing attention as OER catalysts due to their high electrocatalytic activity in alkaline media. LDHs, as a typical brucite-type structure, have been paid great efforts to explore their catalytic performances in OER due to their characteristic structural features (X. Lu et al., 2020; X. Ma et al., 2019). For instance, Ni_2Fe-LDH supported on a conductive carbon fiber showed good activity toward OER with a low overpotential of 289 mV to reach a current density of 10 mA cm^{-2} (η_{10}) and a small Tafel slope of 39 mV dec^{-1} (Zhong et al., 2017). Two dimensional (2D) transition metal oxides with complex metal compositions, such as Fe-Ni, Co-Ni and Fe-Ni-Co oxides possess higher catalytic activities for OER than single iron, nickel or cobalt oxides. For instance, $NiFeO_x$ film presented almost 10 times higher activity in 1 M NaOH than that of CoO_x, and NiO_x, operating at current density of ~3 mA cm^{-2} (Wu, Wang, et al., 2018). $Ni_{0.9}Fe_{0.1}O_x$ thin film with ~2-3 nm thickness showed the most active OER performance in compared with NiO_x, CoO_x, IrO_x, MnO_x, and FeO_x films, requiring an overpotential of 336 mV to drive 10 mA cm^{-2} with Tafel slope of 30 mV dec^{-1} in 1 M KOH (Wu, Wang, et al., 2018). This is because of 2D TMOs with complex metal compositions have higher surface area and nanostructured size than that of single metal oxides, which increases the catalytic activity of OER (Wu, Wang, et al., 2018).

To improve the OER activity of LDH-based materials, various preparation methods have been developed, including exfoliation and doping. Previously, the exfoliation method from top to down has been applied to prepare nanosheets,(X. Lu et al., 2020; X. Ma et al., 2019) nevertheless the high charge density of LDHs seriously hinder the controlled exfoliation process (X. Ma et al., 2019). Additionally, the exfoliation of LDH is commonly a complicated process, which needs lengthy inert environment protection (X. Ma et al., 2019). Metal cation doping has been considered as a promising strategy to boost the intrinsic catalytic activity of the active sites, as it may not only enhance electron transfer during electrocatalysis but also modify the electronic structure of the catalysts that further optimize the reaction energy barrier for the OER. Thus, hydrogen production from water through electrolysis can be made energy and cost-efficient as reported (Sengeni Anantharaj, Kundu, & Noda, 2021). For example, Fe doping has been reported to be effective for improving the catalytic activity of TMOs (Wu, Wang, et al., 2018; Wu, Zou,

et al., 2018) and transition metal phosphines (TMPs) (Septiani et al., 2020). The doping amounts of corresponding cations are essential for enhanced electrochemical performance but it is rarely studied (Y. Li, Dong, & Jiao, 2020). The introduction of active dopants, such as Fe into the NiCo LDH system is expected to enhance the OER activity *via* the creation of vacancies and alteration of the electronic structure of the system (T. Wang, Xu, & Wang, 2017). These events are likely to occur due to the relatively similar ionic size of Fe^{3+} compared to those of Ni^{2+} and Co^{2+} (Septiani et al., 2020), which is the main reason for the selection of iron doping in this work. However, the catalytic performance still needs further improvement, and the preparation of highly active LDH for the electrolysis of water remains as a big issue.

Based on the above-mentioned considerations, Fe-NiCo LDH NSs immobilized on the three dimensional (3D) conductive Nickel foam (NF) (Fe-NiCo LDH/NF) are designed and fabricated as efficient and durable electrocatalysts, which were realized *via* electrochemical deposition method. The electrochemical deposition synthesis is more efficient, simple and time-saving (Guo et al., 2020; Septiani et al., 2020). The proposed strategy is advantageous as it does not involve complex multi-step procedures or complicated template removal process *via* acid/base etching or calcination. When tested for OER, the optimum Fe-NiCo LDH sample (NiCo-4Fe) displays a low overpotential of 189 mV at a current density of 10 mA cm^{-2} and a low Tafel slope of 98.7 mV dec^{-1}. The good OER activity of the as-prepared Fe-NiCo LDH is attributed to (i) the enhanced ion transport and electrical conductivity promoted by iron doping and synergistic effects, and (ii) the provision of many active sites for the OER reactions due to the large specific surface area of the holey nanosheets. Thus, this study provides an effective avenue to fabricate efficient cation-doped multimetallic LDH electrocatalysts for efficient water splitting.

1.2. Statement of the Problem

Due to release of polluted gasses from fossil fuel and shortage of energy, scientists have motivated to search for renewable energy resources that can replace fossil fuels. Still, the large scale production of hydrogen *via* water splitting technology is currently limited by the slow kinetics of the anodic OER which involves a four-step proton-coupled electron transfer (A.-L. Wang et al., 2016). The high cost, rare nature, and poor stability of Ru or Ir based catalysts have impeded their large-scale commercialization. Additionally, other types of synthesis methods (e.g. exfoliation, hydrothermal, co-precipitation) of LDH are commonly complicated process, which

needs lengthy inert environment protection. The synthesis of electrocatalysts for efficient OER by doping using different amounts of corresponding cations/dopants are essential for enhanced electrochemical performance but it is rarely studied (Y. Li et al., 2020). The overall catalytic performance still needs further improvement, and the preparation of highly active NSs for the electrolysis of water remains as a big issue. Herein, we have synthesized Fe-NiCo LDH ultrathin NSs on NF with different Fe dopant content for efficient OER by facile electrochemical deposition method.

1.3. Objectives of the Study

1.3.1. General Objective

The main objective of this work was to study electrochemical synthesis of Fe-NiCo LDH NSs for efficient water oxidation.

1.3.2. Specific Objectives

The specific objectives of this research were:

- ✓ To synthesize Fe-NiCo LDH NSs by electrochemical deposition method.
- ✓ To characterize the synthesized Fe-NiCo LDH NSs using SEM, TEM, HRTEM, AFM, EDS, XRD, and XPS techniques.
- ✓ To probe the electrochemical performance of Fe-NiCo LDH NSs towards OER.

1.4. Significance of the Study

This study area would provide important information about synthesis of Fe-NiCo LDH ultrathin NSs for OER for the production of hydrogen, which will be used as hydrogen fuel. Electrochemical water splitting offers a promising method for large-scale production of hydrogen with zero CO_2 emission, which protects from environmental pollution. The development of electrocatalysts with enhanced kinetics for OER is crucial for accelerating the process of water splitting by lowering overpotentials. Earth-abundant elemental catalysts with comparable catalytic activity are highly desirable to avoid the scarcity and high price of noble metals, such as Ru or Ir based catalysts. The proposed strategy is advantageous as it does not involve complex multi-step procedures or complicated template removal process *via* acid/base etching or calcination. The doping of Fe improves the OER activity by exposing more active

sites. Herein, Fe-NiCo LDH NSs have been synthesized by facile electrochemical deposition method for OER.

1.5. Scope of the Study

The scope of this study was limited to synthesis of Fe-NiCo LDH NSs by using facile electrochemical deposition method, characterization of the Fe-NiCo LDH NSs using SEM, TEM, HRTEM, AFM, EDS, XRD, and XPS techniques, and examination of the performance of Fe-NiCo LDH NSs for OER.

2. LITERATURE REVIEW

2.1. Electrocatalytic Water Splitting

Electrochemical water splitting for large-scale hydrogen production is a potential approach in addressing the issues of energy sustainability. A typical electrolyzer consists of three parts: an aqueous electrolyte, an anode, and a cathode. The bifunctional HER–OER catalysts are applied on both the anode and cathode to speed up the overall water splitting reaction. When an external voltage is applied between the two electrodes, the OER and HER occur at the anode and cathode, respectively (Zou & Zhang, 2015). Depending on the electrolytes in which water splitting proceeds, the water splitting reaction can be described as shown below: (Lasia, 2010)

Total reaction $2H_2O \rightarrow 2H_2 + O_2$ (1)

In acidic solution

Anode $2H_2O \rightarrow 4H^+ + O_2 + 4e^-$ (2)

Cathode $4H^+ + 4e^- \rightarrow 2H_2$ (3)

In neutral or alkaline solution

Anode $4OH^- \rightarrow 2H_2O + O_2 + 4e^-$ (4)

Cathode $4H_2O + 4e^- \rightarrow 2H_2 + 4OH^-$ (5)

Currently, the majority of reported bifunctional HER–OER catalysts work in alkaline electrolytes. Compared to acidic electrolytes, alkaline electrolytes allow for the replacement of precious metal catalysts (Pt, Ir, or Ru based) with inexpensive transition metal and/or functional carbon-based catalysts. In addition, alkaline electrolytes favor the electrocatalytic oxygen evolving process, allowing a significantly faster rate than acidic electrolytes (Z.-L. Wang, Xu, Xu, & Zhang, 2014). The thermodynamic voltage of water splitting is known to be 1.23 V (25 ℃ and 1 atm) regardless of the reaction media (Zou & Zhang, 2015). In order to carry out water splitting at a practical rate, we must apply extra voltages on the cell and the overall operational voltage (V_{OP}) for water splitting can be described as:(Cook et al., 2010)

$$V_{OP} = 1.23\ \text{V} + \eta_a + |\eta_c| + \eta_\Omega \quad (6)$$

where η_{Ω} represents the excess potential applied for compensating the system internal resistance, such as solution resistance and contact resistance. η_a and η_c are the overpotentials required to overcome the intrinsic activation barriers of the anode and cathode, respectively. The intrinsic activation barriers can be minimized by using highly active OER and HER catalysts, respectively. In view of this, the primary challenge for research is to develop efficient bifunctional water splitting electrocatalysts, preferably based on low-cost and earth-abundant elements such that η_a and $|\eta_c|$ are minimized and the water splitting efficiency is improved.

2.1.1. Oxygen Evolution Reaction (OER)

The electrocatalytic water splitting is a simple and effective method to produce high-pure hydrogen through electrochemical splitting of water into hydrogen and oxygen. However, potential scalability is mainly hampered because of the extra overpotential required to drive sluggish OER involving four electron transfers (Hu et al., 2019; Q. Zhao et al., 2018). Most outstanding OER catalysts are based on noble metal oxides such as IrO_2 and RuO_2, which are scarce and costly restraining the achievement of global scalability (Audichon et al., 2016). Several efforts have been devoted to develop an efficient OER catalyst based on earth-abound first-row transition metals (Dionigi et al., 2020) such as Ni, Co, and Fe with promising results using different approaches such as elemental doping (Shin, Xiao, & Goddard III, 2018), defect engineering (R. Liu, Wang, Liu, Zou, & Wang, 2017), and morphology optimization (S. Wan et al., 2017). Among these materials, Ni with other transition metallic oxides and oxyhydrates (Trotochaud, Ranney, Williams, & Boettcher, 2012), sulfides, and nitrides (Nai, Lu, Yu, Wang, & Lou, 2017) have been thoroughly investigated for OER catalysis owing to their remarkable catalytic performance (Tufa, Gicha, Wu, & Lee, 2021).

OER at the anode proceeds through a multistep four-electron transfer process, which is far more complex than the HER at the cathode. The OER mechanisms and reaction pathways are also relatively more complicated than the HER mechanism due to the sluggish kinetics as well. It is worth noting that in the acidic electrolyte, water is oxidized into oxygen and hydrogen ions whereas in the neutral or alkaline electrolyte, the hydroxyl ion is oxidized into water and oxygen. These possible OER mechanisms usually involve three adsorbed intermediates M-OH, M-O and M-OOH on the catalyst surface, whereas the active site is represented as “M” (see Figure 1a) (J. Wang et al., 2020). In the alkaline media, all the proposed mechanisms include the formation of

OH* through an essential elementary step of hydroxide coordination to the active site and the subsequent elementary step of the formation of other intermediates. Irrespective of the reaction conditions, there are the same intermediates such as OH* and O* among the proposed OER mechanisms, whereas the formation of oxygen is likely to be the main difference. Based on the theoretically proposed models, the widely accepted mechanisms for the OER under the acidic and alkaline conditions can be separately expressed as follows:(J. Wang et al., 2020)

OER in the acidic electrolyte

$$H_2O + * \rightarrow HO* + H^+ + e^- \quad (7)$$

$$HO* \rightarrow O* + H^+ + e^- \quad (8)$$

$$O* + H_2O \rightarrow HOO* + H^+ + e^- \quad (9)$$

$$HOO* \rightarrow * + O_2 + H^+ + e^- \quad (10)$$

OER in the alkaline electrolyte

$$OH^- + * \rightarrow HO* + e^- \quad (11)$$

$$HO* + OH^- \rightarrow O* + H_2O + e^- \quad (12)$$

$$O* + OH^- \rightarrow HOO* + e^- \quad (13)$$

$$HOO* \rightarrow * + O_2 + H_2O + e^- \quad (14)$$

where * denotes the active site of catalyst, OH*, O*, and OOH* represent adsorbed intermediates species.

LDHs recently attracted considerable research interest owing to their intriguing electrocatalytic activities, earth abundance, ultrastability, and low-toxic properties (X. Lu et al., 2020). LDHs can be represented by a general formula as $[M_{1-x}^{2+}M_x^{3+}(OH)_2]A_{x/m}^{m-}.nH_2O$ (X. Lu et al., 2020). Where M^{2+} and M^{3+} are divalent and trivalent cations and A^{m-} represents an anion with an m-charge and x usually has a value between 0.25 and 0.33. As depicted in Figure 1b, LDHs consist of brucite-like layers with a fraction of octahedrally coordinated divalent metal cations replaced by trivalent ones, resulting in positive charge of the host layers. Moreover, the hydroxyl groups

of the host layers are connected to the anions or water molecules by hydrogen bonds. X. Ma *et al.,* successfully synthesized one-pot synthesis of NiCo LDH as efficient catalysts for OER. During the OER catalytic process, both M^{2+} and M^{3+} are involved in redox reactions by adsorbing and desorbing reactants, intermediates, and products (Figure 1a). There may be possible electron transfer occurring between M^{2+} and M^{3+} in the process. $A^{m/n-}$, acting as the counter ions to compensate for the positive charge, may affect adsorption/ desorption process on LDH host layer surface and/or in the interlayer space (X. Ma et al., 2019). The lateral size and thickness of LDHs have a great effect on physical and chemical properties (X. Ma et al., 2019). In particular, when the thickness reduced to nanometer or even molecular scale, the resulting nanosheets can maximize the exposing active sites and specific surface area, which would effectively contribute to increased intrinsic electrocatalytic activities, facilitate the transport of reactant species, and finally promote the activity toward water splitting (X. Ma et al., 2019). Herein, we have synthesized Fe-NiCo LDH NSs for efficient OER by electrochemical deposition method. The Fe-NiCo LDH ultrathin NS is used for as a catalyst for OER. Remarkably, the ultrathin structure could expose more active sites, and the doping of Fe^{3+} could also tune the electronic structure of LDH, thus improving the activity of active sites.

Despite the enormous progress made so far, there is still a controversy on elucidating the actual role of Fe specifically with regard to its position within the main catalyst part (Gicha, Tufa, Choi, & Lee, 2021a). It is well acknowledged that doping of Fe to Ni-based catalyst is a well-established means to improve their intrinsic activities toward OER catalysis (Gicha, Tufa, et al., 2021a). Friebel *et al*., described that Fe ion was deposited as an active site in $Ni_{1-x}Fe_xOOH$ where Fe^{3+} occupies octahedral sites, resulting in a short Fe−O bond distance to enhance the binding energies of intermediates during the OER reaction (Friebel et al., 2015). Louie *et al.,* have also indicated that Ni−Fe films with ∼40% Fe composition induced 2−3-fold activity enhancement compared with pure Ni and Fe films, where the activity enhancement was attributed to change in the redox properties of Ni from the presence of Fe (Louie & Bell, 2013). Martirez and Carter have also reported a lower overpotential of 140 mV for Fe-doped β-NiOOH compared to 490 mV for pure NiOOH, describing that the activity difference is owing to surface oxidization of Fe^{3+} to iron(IV)-oxo species (Martirez & Carter, 2018). The importance of Fe-doping is to enhance catalytic activity during the synthesis of NiCo LDH NSs. Therefore, understanding the role of Fe with regard to its position within the main catalyst part and

synergetic effect between different positions toward promoting OER catalysis is paramount to develop an efficient electrocatalyst.

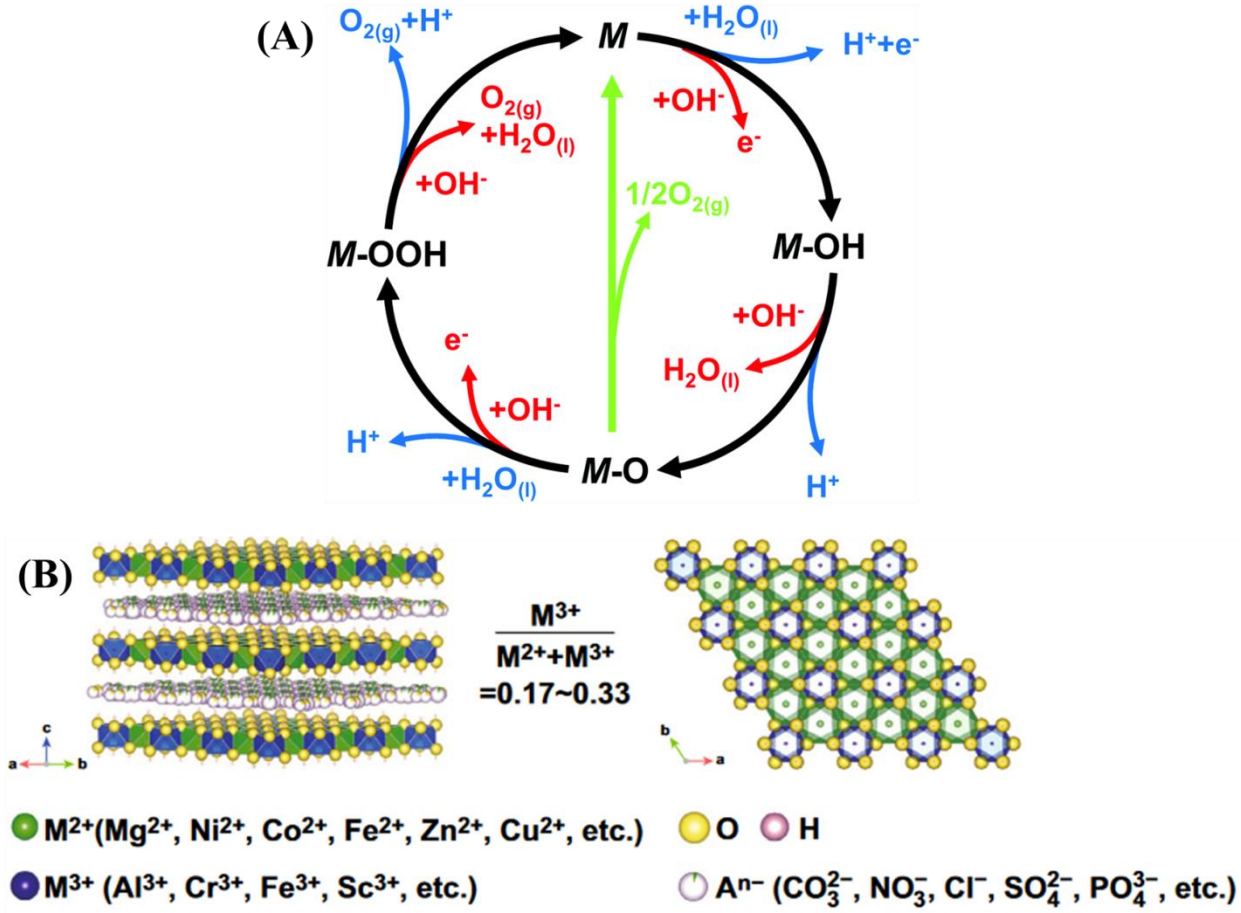

Figure 1: a) OER mechanisms in acid (blue) and alkaline (red) conditions (J. Wang et al., 2020). (b) Typical structure model of LDHs and in-plane cation arrangement (X. Lu et al., 2020). Copyright (2020), Springer.

2.1.2. Evaluation Parameters for OER

For any given electrocatalyst, the most desired characteristics are high activity (both thermodynamic and kinetic), reasonable stability and high selectivity (Sengeni Anantharaj & Noda, 2020; Z. Zhao et al., 2019). The same is applicable to the electrocatalysts of OER too. Activity of an electrocatalyst is screened by various methods based on various parameters. Important ones are overpotential at a defined areal current density (usually at 10 mA cm^{-2}), overpotential at a defined mass normalized current density, overpotential at a defined electrochemical surface area (ECSA) normalized current density, Tafel slope, exchange current

density, and turnover frequency (TOF). Among these, the last three are kinetic activity parameters that tell us how fast the reaction is occurring. As far as overpotential is considered regardless of current normalization method, it should be as low as possible. However, the practice of using overpotential at 10 mA cm^{-2} is being followed as an engineering perspective of the prepared electrode (Sengeni Anantharaj & Noda, 2020). Similarly, the mass activity (overpotential at a defined mass normalized current density) is also adapted sometimes by researchers to show the catalyst loading effect. Unfortunately, both areal (overpotential at a defined geometrical area normalized current density) and mass activities cannot reflect the intrinsic activity unlike the specific activity (overpotential at a defined ECSA normalized current density). An excellent electrocatalyst should possess high catalytic activity that can reduce the overpotential in the catalytic process and increase the current density per unit mass. Overpotential is the activity parameter which is treated as the most important (Sengeni Anantharaj & Noda, 2020; Walter, Menezes, & Driess, 2021). However, it is complex to understand the real meaning of overpotential at a defined current density, which is greatly different from the iR-compensated overpotential ($\eta_{iR\ free}$) at a defined current density. Before differentiating these in detail, overpotential should first be defined. Overpotential of any electrochemical process can be defined as the additional potential required to sustainably drive an electrochemical reaction from its reversible potential (S Anantharaj et al., 2018; Walter et al., 2021). The reversible potentials for OER is 1.23 V vs. standard hydrogen electrode (SHE). Hence, the equations $\eta_{OER} = E_{RHE}$ - 1.23 V can be used for OER to calculate overpotentials at a desired current density without iR compensation (Gicha, Tufa, Choi, & Lee, 2021b). The main parameters for the evaluation of the performance of electrocatalysts in the electrochemical water splitting are indicated in Table 1.

Table 1: Evaluation parameters for OER and their applications.

Parameter	Formula/equation	Uses	Ref.
Overpotential (η)	$\eta = E - E_{eq}$	Directly restricts the energy efficiency of water splitting. Essential to drive the electron transfer processes at a desired rate.	(Z. Cai et al., 2019)

Tafel slope (b)	$\eta = a + b\log(j)$	Shows how efficiently an electrode can produce current in response to change in applied potential. To deduce the possible kinetic rate of the electrocatalyst and determine the reaction mechanism.	(Gicha, Tufa, Kang, et al., 2021)
Turnover frequency (TOF)	$TOF = \frac{(J)(A)}{4(F)(m)}$	Deduce the intrinsic activity of each catalytic active site under the defined reaction conditions.	(Z. Cai et al., 2019)
Stability	Measured by CA, CP, CV and LSV	To assess the ability of a catalyst to maintain activity with a long-term operation period.	(J. Wang et al., 2020)
Faradaic efficiency (FE)	$FE = \frac{I_R n_D}{I_D n_R N_{CL}}$	It is important that the electrons added to an electrolyzer are used to drive the water-splitting reactions.	(Sengeni Anantharaj et al., 2016)
Electrochemical surface area (ECSA)	$ECSA = \frac{C_{dl}}{C_s}$	To determine quantitatively the reacting interface of a given catalyst.	(Z. Cai et al., 2019)

Note: Where η (overpotential), E (applied potential), E_{eq} (equilibrium potential), j (current density), A (surface area), F (faraday constant), m (number of moles of the active materials), CV (Cyclic voltammetry), LSV (Linear sweep voltammetry), CA (Chronoamperometry), CP (Chronopotentiometry), I_R and n_R (current and the number of electron transfer at the ring, respectively); I_D and n_D (current and the number of electron transfer at the disc, respectively); N_{CL} (collection efficiency of the rotating ring disc electrode used), C_{dl} (electric double layer capacitance), and C_s (specific capacitance).

2.2. Ni-based LDH NSs

Metal foam is a cellular structure consisting of solid metal with gas-filled pores comprising a large portion of the volume. As a 2D material, the metal foam was often considered as a

promising substrate to combine with Ni-based LDH NSs for the robust catalyst fabrication. The metal foams often have high conductivity and large space to anchor Ni-based LDHs to form the well-defined porous nanostructure, which can effectively make the entire catalysts accessible to the electrolyte and reduce the "dead surface" (L. Yang, Liu, Zhu, Feng, & Xing, 2021). The porous nanostructure can efficiently promote ion diffusion and enhance OER catalytic performance. Besides, Ni-based LDHs on the metal foam can be directly used as the electrode without the need for a binder to immobilize. The absence of the polymer binder in the catalysts system can avoid the electrical resistance caused by the binder and decrease the damage of the porous nanostructure. For example, nickel foam has been generally employed as a conductive substrate to anchor Ni-based LDHs (L. Yang et al., 2021). Among these, the Cr^{3+} incorporated Ni-based LDHs have attracted great attention, by tuning the ratios of Ni/Cr to get the optimized Ni_2Cr_1 LDH on the Ni foam, an outperforming activity was found for water oxidation reaction with a rather low overpotential of 319 mV at 100 mA cm^{-2} (L. Yang et al., 2021). A dissolution-precipitation mechanism was proposed for the fabrication of NiFe LDH electrocatalyst on the Ni foam (H. Yang, Wang, Zhang, & Wang, 2019). The hydrolysis of Fe^{3+} could etch Ni foam to generate Ni^{2+} in the acid conditions, and the obtained Ni^{2+} and hydrolyzed Fe^{3+} was co-precipitated to grown NiFe LDH on the Ni foam.

Specifically, benefiting from earth-abundance, corrosion resistance and good ductility of nickel, Ni-based NSs (such as NiFe-LDH (Gong et al., 2013), Ni-Co-Fe based mixed sulfide (Darband, Aliofkhazraei, Hyun, Rouhaghdam, & Shanmugam, 2019), NiCo-LDH (W. Liu et al., 2017), $Ni_{1-x}Fe_x$ Oxyhydroxide (Gicha, Tufa, et al., 2021b), NiMn-LDH (Sumboja, Chen, Zong, Lee, & Liu, 2017), Fe_x-NiCoP (Guo et al., 2020), and NiCr-LDH (Ye, Fang, Chen, & Yan, 2018) etc.) have been the subject of deep investigation in the recent years especially for electrochemical water splitting. Subbaraman *et al*. have reported on 2D transition-metals (Ni, Co, Fe, Mn) hydr(oxy)oxide for OER and discovered that the excellent OER activity followed the same trend (Ni > Co > Fe > Mn) as observed in perovskite systems (Subbaraman et al., 2012). Dai *et al.* synthesized ultrathin $Ni/Ni(OH)_2$ NSs for overall water splitting with low overpotentials of 77 and 270 mV for HER and OER at current density of 10 mA cm^{-2} respectively (Dai et al., 2020). The lower overpotential enhances the catalytic activities of overall water splitting. The poor conductivity is one of the biggest obstacles, which prevents the catalysts from reaching extremely high activity and prolonged stability. To overcome these limitations, the growth of Ni-

based LDH NSs on the conductive substrates (such as NF, carbon nanotubes, etc.) provides an effective way to enhance conductivity in OER (Dai et al., 2020). However, the overall catalytic performance still needs further improvement, and the preparation of highly active Ni-based LDH NSs for the electrolysis of water remains as a big issue (Ahn & Manthiram, 2020).

In a short summary, the enhanced OER performance of the metal foam/Ni-based LDHs composites can be attributed to the following reasons: 1) the porous structure of the metal foams can anchor more Ni-based LDHs tightly on the surface to expose more active sites; 2) The Ni-based LDHs deposited on the metal foam without using binder can decrease the resistance between the interface and facilitate the electron transport; 3) the synergistic effect between the conductive metal foam and active phases of Ni based LDH NSs accelerate electrocatalytic process *via* charge transfer; 4) the 2D structure of the metal foam makes the electrolyte easily accessible to the entire catalysts to favor the catalytic performance of the OER (L. Yang et al., 2021). Herein, we demonstrated the construction of Fe-NiCo LDH ultrathin NSs on NF with different Fe dopant content *via* a facile electrochemical deposition method for OER. Remarkably, the ultrathin structure of Fe-NiCo LDH could expose more active sites, and the doping of Fe^{3+} could also tune the electronic structure of LDH, thus improving the activity of active sites.

2.3. Effect of Fe-doping in Ni-based LDH NSs

It is well-known that Fe^{3+} is the strongest transition metals based Lewis acid which found enormous use in the organic transformation particularly in aromatic electrophilic substitution reactions in aryl rings. Such a high electrophilic nature of Fe^{3+} must also possess notable effect in altering the electronic properties of other cations of the host material into which it is being incorporated. According to Li *et al*., (N. Li et al., 2017) Fe^{3+} ions with the pKa of 2.2 increases the acidity of the hydroxyl proton that is coordinated to the Ni site which upon polarization undergoes oxidation with a relatively lower activation threshold. This led to the formation of increased amount of Ni^{4+} cations which in turn directly correlated to the enhanced OER activity. On the other hand, the same Lewis acidic character of Fe^{3+} ions can also be attributed to the anodic shift of oxyhydroxide formation peak in Ni and Co based oxygen-evolving catalysts (OECs). It is because, as Fe^{3+}–O is relatively more ionic than Ni^{2+}–O and Co^{2+}–O bonds, they become more covalent when Fe^{3+} ions are getting incorporated into their lattices. Due to this

increased covalent character in Ni^{2+}–O and Co^{2+}–O bonds, their electrochemical oxidation requires addition potential which is the reason why we observe an obvious anodic shift in the oxyhydroxide formation peaks of Ni and Co based OECs with Fe incorporation and with its increasing amount. These two observations suggest an important thing here which are; 1) the kinetically competitive metal oxidation reaction is suppressed by Fe^{3+} incorporation and 2) in the meantime, the same Fe^{3+} incorporation increases the population of Ni^{4+} which would result in enhanced OER (by increasing the kinetically competitive Ni^{4+} reduction reaction)

Undoubtedly, it is true that incorporation of Fe has been being the reason behind the substantial OER enhancements witnessed with Ni based LDHs in unpurified, reagent grade KOH so far. Researchers have reported the OER activities of these materials without knowing the fact that Fe in less than 1 ppm concentration could also alter the OER activities of Ni based LDHs dramatically (Sengeni Anantharaj et al., 2021). Based on these facts several studies were reported in literature describing different roles for Fe in Ni based LDHs' matrices (Görlin et al., 2017; Klaus, Cai, Louie, Trotochaud, & Bell, 2015). Important roles that are stated in literature with experimental evidences are; 1) Fe increases the conductivity (Klaus et al., 2015), 2) Incorporation of Fe in place of Ni and Co in their respective (oxy)hydroxide matrices make them harder to oxidize further and thus alters the redox electrochemistry of Ni and Co (Görlin et al., 2017), 3) Fe induces the structural transformation upon incorporation into Ni (oxy)hydroxides (Görlin et al., 2017), 4) As incorporated Fe^{3+} is the strongest transition metals based Lewis acid, it assist the formation of active Ni^{4+} sites (Sengeni Anantharaj et al., 2021), and 5) Fe^{3+} ions in NiFe (oxy)hydroxide with the ratio of 1:0.33 shows superexchange magnetic interaction which enhances the OER electrocatalysis through electron hopping (Klaus et al., 2015).

Metal cation doping has been considered as a promising strategy to boost the intrinsic catalytic activity of the active sites, as it may not only enhance electron transfer during electrocatalysis but also modify the electronic structure of the catalysts that further optimize the reaction energy barrier for the OER. The doping of Fe improves the OER activity by exposing more active sites. Thus, hydrogen production from water through electrolysis can be made energy and cost-efficient as reported (Sengeni Anantharaj et al., 2021). For example, Fe doping has been reported to be effective for improving the catalytic activity of TMOs (Wu, Wang, et al., 2018; Wu, Zou, et al., 2018) and TMPs (Septiani et al., 2020). In this part of the Literature review, all these

reported roles are critically discussed and summed up to give a clear-cut understanding on “the Fe effect”.

2.4. Typical Synthetic and Fabrication Methods of Ni-based LDH NSs

Nanosheets (NSs) have attracted significant interest for electrocatalytic applications owing to their high surface-to-volume ratio and unique physical, chemical, and electronic properties (Septiani et al., 2020). These attractive features lead to more exposed active sites and improved mass or ion transport, which are beneficial for enhancing the electrocatalytic activity due to their unique properties originating from their ultrathin thickness (Dai et al., 2020). Many synthesis methods of the Ni-based NSs have been reported, and they mainly include solvothermal (hydrothermal) method, co-precipitation method, electrochemical deposition method, and etc. In order to further understand the influence of the synthesis methods on the structure and composition of the Ni-based NSs, we introduce some common synthesis methods as follows.

2.4.1. Hydro/Solvothermal Synthesis Method

Hydrothermal synthesis is usually conducted in a sealed container such as a Teflon-lined autoclave to allow the aqueous solution containing metal ions and anion precursors to be placed under high-temperature and vapor pressure. The only difference between solvothermal synthesis and hydrothermal synthesis is that other solvents or organic solvents are used instead of water in the former process. These methods can be extended to induce hybridization with metal compounds and carbonaceous materials, as well as the synthesis of various ultrathin NSs. This method is a simple yet efficacious way to fabricate Ni-based ultrathin NSs with controlled compositions and structures, and it can be easily realized *via* adjusting the metal salt precursors and temperature/pressure conditions. Dutta *et al.* fabricated a self-supported NiFe LDH-NiSe electrocatalyst by stepwise surface-redox-etching of NF through a hydrothermal process (Dutta, Indra, Feng, Song, & Paik, 2017). In this typical procedure, aqueous solution containing of iron chloride ($FeCl_3.6H_2O$), ammonium fluoride (NH_4F) and urea were prepared first and then the as-prepared $NiSe_x$/NF was immersed into it. Finally the whole mixture was hydrothermally treated in a Teflon-lined stainless steel autoclave for 5 h under 100 °C. The final product was washed thoroughly with deionized water and dried at 60 °C overnight before further use. Yuan *et al.* reported the direct growth of Fe-doped Ni_3S_2 NS arrays on a conductive Fe–Ni alloy foil *via* a

one-step solvothermal method (Yuan et al., 2017). A piece of Fe-Ni alloy foil was immersed into a mixture of Na_2S solution and ethanol, and this was then transferred into a Teflon-lined stainless-steel autoclave under N_2 flow. The reaction was carried out at 200 ℃ for 12 h in an electric oven and the obtained Fe-doped Ni_3S_2 NSs grown in situ on the surface of the alloy foil could be applied as a self-supported electrode for water oxidation.

NSs obtained by this method can be a single component or a multicomponent. Furthermore, the method can prepare some particles with uniform size, high purity, good dispersion, and unique crystal shape. Ahn *et al.* (Ahn & Manthiram, 2020) supported NiFe-imidazole salt complex on NF by hydrothermal synthesis method, then prepared M–N–C catalyst on NF at 700 ℃ with melamine as carbon source. The electrode had excellent catalytic activities for HER and OER. During the hydrothermal synthesis process, 2D NiFe iron hydroxide NSs were grown at 180 ℃ on the NF. NF provided the growth substrate, whereas one dimensional (1D) microfibers continued to grow on the generated polygon 2D NS to form 2D/1D NS. This unique structure largely reduces the interface resistance, increases the ECSA, and displays superior HER and OER catalytic activities. It shows that hydrothermal synthesis can synthesize different types and structures of catalysts by adjusting synthesis conditions.

The morphology and structure of the materials can be easily manipulated by changing temperature, time, and solvent (L. Yang et al., 2021). As key reaction factors in the solvothermal method, the solvent, and precursor concentration exhibit great effects on the structural modification of Ni-based ultrathin NSs. It has been reported that the formation of Ni-based LDHs *via* solvothermal method is the aggregation-based (nucleation – dissolution - recrystallization aggregation - solid phase transformation) mechanism instead of the ion-by-ion mechanism (Sun et al., 2019). The formation of the initial LDHs crystallite nuclei is crucial because it will impinge on adjacent crystals and determine the direction of crystal growth (L. Yang et al., 2021). Thus, urea, hexamethylenetetramine (HMTA), cetyltrimethylammonium bromide (CTAB) and hexamine as hydrolytic reagents and alkali sources are applied to trigger the formation of homogenous nucleation and promote the crystallization of LDHs (L. Yang et al., 2021). Besides, some surface energy modifiers such as H_2O and anions can impact the growth of the crystals to some degree by adsorption on crystallographic planes. For example, NiFe LDHs hollow microspheres were fabricated by the hydrothermal treatment and discovered

that the different concentrations of NH_4F led to the diversity of the morphology. When the concentration of NH_4F changed from 0 M to 0.2 M, the NiFe-LDHs hollow microspheres tended to form (Zhong et al., 2019).

The temperature and time also played an important role in the catalytic activity of Ni-based ultrathin NSs. Muhammad *et al.* constructed NiMn-LDH/g-C_3N_4 by hydrothermal treatment at different temperature of 100 ℃, 150 ℃, 180 ℃ and 200 ℃ for 12 h and discovered that the optimized material was synthesized at 180 ℃ (Shakeel, Arif, Yasin, Li, & Khan, 2019). Adjusting the ratio of metal ions and concentration by one-step hydrothermal method, different crystal morphologies and properties of NiCo-LDHs can be obtained (Jing et al., 2018). The surface structure can also be changed by choosing the different surfactants via the hydrothermal method; a laminar structure NiFe-based LDHs was reported by using the sodium dodecyl sulfate as a surfactant (H. Zhang, Li, Akram, & Wang, 2019). Moreover, the FeNi-LDHs arrays on the Ni foam fabricated by a two-step hydrothermal approach were reported to have a rougher surface and larger active area than the one-step hydrothermal method (Huang et al., 2019). The solvothermal method is a handy and relatively mature approach to synthesizing and manipulating Ni-based ultrathin NSs, However, the disadvantage is that the hydrothermal synthesis method requires high material demands for the reaction vessel (hydrothermal kettle). In addition to high temperature and pressure resistance, it cannot react with water and system media, so it is generally made of polytetrafluoroethylene (PTFE).

2.4.2. Co-precipitation Method

The co-precipitation method is the most widely used method for the synthesis of Ni-based ultrathin NSs. In this method, a mixed solution of di and trivalent metal ions is slowly added to another solution which is alkaline in nature at a selected pH, which leads to the precipitation of two metallic salts (Karmakar et al., 2021). Often, Co-precipitation is coupled with the hydrothermal method to increase the yield of a product, to control the size of the particles and also to improve its crystallinity. There are many factors that influence the synthesis of Ni-based ultrathin NS with control over size, high surface area, high porosity and high purity. The crystallinity and especially the purity of the Ni-based ultrathin NSs are highly dependent on the pH of the medium. For example, in the synthesis of NiFe-LDH by urea hydrolysis, if the pH of the medium is higher than 12, then the formation of β-$Ni(OH)_2$ is the major process, which will

affect the properties of LDH (Karmakar et al., 2021). Qian *et al.* prepared trimetallic NiCoFe ultrathin NS *via* one-pot co-precipitation. In particular, they added a pre-oxidation step with H_2O_2 solution to induce the partial conversion of Co^{2+} to Co^{3+}. Then, the solution of Ni^{2+}, Co^{2+}, Co^{3+}, and Fe^{3+} was mixed with another solution containing 1 M NaOH and 0.1 M Na_2CO_3 to adjust the pH of the solution to 8.5, and the resultant solution was stirred for 4 h to yield NiCoFe ultrathin NS (Qian et al., 2015). Lu *et al.* also synthesized NiFeMn NS under a very similar reaction condition using NaOH and Na_2CO_3 (Z. Lu et al., 2016).

Ni-based NSs synthesized by co-precipitation method often have high purity and crystallinity since low temperatures can maintain the (oxy) hydroxide but it is poor to control the morphology. Different ratios of metal salts (metal sulfates, metal nitrates, metal chlorides *et al.*) are acted as the precursor and accompanied by precipitating agents. Wang *et al.* were able to synthesize RuNiFe, RuNiAl, and RuMgAl LDHs via a one-step co-precipitation procedure (Zelin Wang et al., 2019). A solution containing all three metal precursors was added to an aqueous solution of $NaNO_3$ and 23 vol% formamide. Then, a NaOH solution was added to adjust the pH to 10 at 80℃. The reaction was complete after 10 min. The most common precipitating agent is sodium hydroxide and it is often accompanied by sodium carbonate. The concentration of the alkaline solution affect the formation of the ultrathin NSs (L. Yang et al., 2021). For example, Ce-doped NiFe-NSs has been successfully prepared by a convenient and low-cost precipitation method in which NaOH (0.012 M) and Na_2CO_3 (0.03 M) were applied as an alkaline solution, whose concentration was higher than the total metal salts (6 mM) (H. Xu et al., 2018). Besides, ammonia can also be considered as an ideal precipitation agent to form the nitrate forms of NSs rather than the carbonate forms (L. Yang et al., 2021). But the possibility of the formation of ammine complexes should be excluded when applying this synthetic method. Urea solution, which can release hydroxide ions by hydrolyzing, can also act as the precipitation agent, while its application is extremely limited because the reaction temperature has control over the precipitation process (L. Yang et al., 2021). Some other factors such as nature of the alkaline solution, aging time and aging temperature, metal molar ratios should also be considered when fabricating Ni-based ultrathin NSs by co-precipitation method.

The co-precipitation is a rather direct and ahead method compared with others. For example, Wang *et al.* report a NiV LDH ultrathin NS doped with Fe^{3+} through a one-step co-precipitation

method. A low overpotential of 269 mV was required achieving the current density of 10 mA cm^{-2} and a long-term stability for 1000 cycles was also shown for the obtained electrode, which has higher catalytic performance (Zhaolong Wang et al., 2019). Also Yan *et al.* presented a facile co-precipitation method to prepare Ni-based ultrathin nickel-cyanide coordination polymer nanosheets. The Ni_3C based NSs have lateral length of about 200 nm and thickness of 10 nm. When doped with Fe, the Ni_3C based nanosheets exhibited outstanding electrocatalytic properties for both HER and OER. For example, 2 % Fe (atomic percent) doped Ni_3C nanosheets depict a low overpotential (292 mV) and a small Tafel slope (41.3 mV dec^{-1}) for HER in KOH solution. An outstanding OER catalytic property is also achieved with a low overpotential of 275 mV and a small Tafel slope of 62 mV dec^{-1} in KOH solution (Fan et al., 2017). Such NSs incorporated 2D ultrathin hybrid structures can serve as an efficient bifunctional electrocatalyst for overall water splitting.

In summary, it is a suitable method to construct highly active electrocatalyst with alloying effects, heterostructures, and so on due to the facile controllability of the co-precipitation method. The catalyst synthesized by this method can display superior activity and relatively low industrial production cost. However, it could be noted that the concentration of metal precursors, heating rate, reaction temperature should be precisely regulated.

2.4.3. Electrochemical Deposition Method

Electrochemical deposition is widely adopted technique used to prepare various nanostructured materials. It requires the use of a conductive substrate as a working electrode. Typically, a three-electrode system is prepared in an aqueous solution with metal precursors. Then, Ni-based ultrathin NSs are synthesized on the working electrode either at a constant potential or by sweeping a specific range of potential. The advantage of the electrodeposition method is that, in most cases, no additional reagents besides the metal precursors are required to induce the formation of ultrathin species. During the electrodeposition process, water molecules are electrolyzed to produce oxygen gas and hydroxide ions, which facilitates the formation of metal hydroxide species. Kim *et al.* prepared NiFeCo LDH nanosheet arrays on NF (Babar et al., 2019). In this case, they prepared an aqueous solution of Ni, Fe, Co chloride precursors, and conducted cyclic voltammetry (CV) in the potential range between -0.4 to -1.3 V for 10 cycles. Darband *et al.* studied, firstly, Ni nanocones (NNCs) were formed using electrochemical

deposition, and then Ni-Co-Fe based mixed sulfide ultrathin nanosheets were obtained by directly depositing on the surface of the NNCs using the CV method for electrochemical water splitting (Darband et al., 2019). Yang, R., *et al.* synthesized a hierarchical CoFe@NiFe/NF core-shell architectures in two step process (R. Yang et al., 2019). Firstly, the CoFe-LDH nanosheet arrays were synthesized on the NF substrate *via* a facile hydrothermal method. Subsequently, the NiFe-LDH NS was decorated on the CoFe-LDH NS arrays by a fast electrodeposition method, forming the hierarchical CoFe@NiFe/NF core-shell architectures. After electrodeposition, the NiFe-LDH NSs were erectly deposited on the CoFe-LDH NS arrays substrate, forming well-defined hierarchical "NS on NS" architecture. This hierarchical "NS on NS" architecture not only provides enlarged surface area with more active sites for the redox reactions, but also possesses open porous structure that can facilitate the fast mass transport and electrolyte penetration; therefore endowing the electrodes with high electrocatalytic performance.

By adjusting the potential or current density in the electrochemical deposition process, the catalyst can be finely regulated. There have been some reports of electrodeposited Ni-based ultrathin NSs for electrochemical water splitting. For example, Cao *et al.* synthesized 3D petal-like clusters constructed by cross-linking 2D ultrathin nickel hydroxide NSs with size of ∼3.0 nm on NF by using a relatively high electrodeposition potential, which required an overpotential of 192, 240, and 290 mV to yield current densities of 10, 100, and 250 mA cm^{-2} in 1.0 M KOH, respectively (Cao et al., 2021). Moreover, α- $Ni(OH)_2$/NF can even drive the high current density (500−1000 mA cm^{-2}) at low overpotentials, indicating that it has potential industrialization prospects. The Tafel slope of the α-$Ni(OH)_2$/NF electrode is 108 mV dec^{-1}, being much lower than those of RuO_2/NF (126 mV dec^{-1}) and NF (170 mV dec^{-1}), suggesting fast catalytic kinetics of α- $Ni(OH)_2$/NF for OER. Geng *et al.* synthesized α-$Ni(OH)_2$ NSs on a NF/N-CNT (carbon nanotubes) substrate *via* electrodeposition under a constant cathodic current of 2 mA cm^{-2}, which required an overpotential of 254 mV to yield a current density of 10 mA cm^{-2} in 1.0 M KOH (Wu, Wang, et al., 2018).

The size of the conductive substrate, the concentration of the metal salts, deposition voltage and the time of the electrochemical deposition can have great control over the mass and the quality of the products. For example, Liu *et al.* have successfully deposited a hierarchical NiCo@NiCo

LDH core-shell nanotube array on carbon fiber cloth (CFC) via two-step electrodeposition followed by the removal of the ZnO template in NaOH solution under the same condition except for the molar concentrations of Co^{2+}: Ni^{2+} in the solution (Y. Liu et al., 2017). Zhang *et al.* electrochemically deposited single-atom Au on NiFe LDH using Ti mesh as a working electrode (J. Zhang et al., 2018). The electrodeposition of Au was carried out by stepping the potential to -0.6 V vs. saturated calomel electrode (SCE) for 5 seconds, followed by stepping back to -0.2 V vs. SCE for 5 seconds for five cycles. The heterostructure of electrodeposited NiFe-LDHs NS array on the surface of CoFe-LDHs supported on NF realized high OER activities and stability (R. Yang et al., 2019). Therefore, the exploration of the optimized size of the conductive substrate, the concentration of the metal salts and the voltage and the time of the electrochemical deposition are required when using the electrochemical deposition method.

In conclusion, electrochemical deposition method is a controllable, simple, eco-friendly and low-cost approach to prepare catalysts for water splitting, which can fabricate some unique structure catalysts. Simultaneously, electrochemical deposition has also been proved to be a general and efficient synthetic means to synthesize monatomic catalysts (W. Liu, Cao, & Cheng, 2021). However, electrochemical deposition still has some disadvantages. The deposition efficiency is always affected by the electrode polarization and solvent effect derived from the charge transfer and concentration gradient in the solution.

2.4.4. Other Methods

Apart from the commonly employed methods mentioned above, there are still some convenient methods to synthesize Ni-based ultrathin LDHs. The topo-chemical transformation method can be applied to fabricate the TM-LDHs with high crystallinity since it can control the oxidation states of the transition metal in the hydroxide precursor well (R. Ma et al., 2007). Besides, the one-pot anion exchange intercalation method has been considered as an alternative way to exchange the anions or molecules between the layers. Lv *et al.* have intercalated glucose into the NiMn LDHs nanosheets to expand the interlayer distances and optimize the electrochemical performance of NiMn LDHs NSs, breaking the bottleneck of the rational design of the Ni-based LDHs (Lv et al., 2016). The mild microwave assisted hydrothermal method was reported to promote the hollow spherical Al_2O_3 NSs template without any damage transformed into NiAl-LDHs NSs (L. Yang et al., 2021). Furthermore, some methods, like liquid-phase exfoliation

method, corrosion engineering method, ion-exchange method and reverse microemulsion approach, have recently emerged out to fabricate monolayer Ni based LDHs, which can inhibit from aggregation and offer easy accessibility to the interlayer active sites of the LDHs.

By considering all the aspects mentioned above, we have synthesized Fe-NiCo LDH NSs on NF by a facile electrochemical deposition method for efficient OER.

3. MATERIALS AND METHOD

3.1. Study Site Description

Synthesis of Fe-NiCo LDH NSs was conducted at the electroanalytical laboratory of Adama Science and Technology University at the Department of Applied Chemistry. XRD characterization of the synthesized NSs was conducted at Adama Science and Technology University at the Department of Material Engineering and SEM, TEM, HRTEM, AFM, EDS, and XPS characterizations were done at Chungnam National University, South Korea. The electrochemical water splitting was conducted at the electroanalytical laboratory of Adama Science and Technology University in the Department of Applied Chemistry.

3.2. Chemicals and Reagents

NF (purity > 99.99%; surface density 346 g/cm^2; and thickness 1.6 mm) and FTO (purity 99.99%) obtained from MTI Korea Inc.; HCl, 37%, Ni $(NO_3)_2 \cdot 6H_2O$, 99.999%, Co $(NO_3)_2 \cdot 6H_2O$, 99.999%, and $FeSO_4.7H_2O$, 99.95% trace metal basis, KOH ACS reagent ≥85% pellets purchased from Sigma-Aldrich; and distilled water obtained from Adama Science and Technology University at Department of Applied Chemistry; were used in this work. All chemicals were used without any further purification.

3.3. Synthesis of Fe-NiCo LDH NSs Electrocatalysts

The Fe-NiCo LDH NSs were prepared by a two-step electrochemical deposition method. The Synthesis of Fe-NiCo LDH NSs on NF was carried out according to the recently reported literature with a slight modification (Gicha, Tufa, et al., 2021a). Prior to the deposition, the NF (20 mm length x 10 mm width x 1.6 mm thickness) was sonicated with 1 M HCl for 30 min to remove the oxide layer. Then, the HCl soaked NF was air dried to remove the moisture. The electrochemical deposition was performed in a three-electrode cell using the NF (size 1 cm x 1 cm) as the working electrode, platinum wire as the counter electrode, and Ag/AgCl electrode as the reference electrode. In the first step process, a voltage of -1.0 V was applied for 300 s in the electrolyte containing 6 mM of Ni $(NO_3)_2 \cdot 6H_2O$ and Co $(NO_3)_2 \cdot 6H_2O$. Then, the targeted NiCo LDH NSs were rinsed and air dried for 8 h. In the second step, different amounts (2, 4, 6, and 8 mM) of $FeSO_4.7H_2O$ solutions were doped on NiCo LDH electrode by CA at a voltage of -1.0 V

for 300 s. After the deposition, the as-prepared Fe_x-NiCo LDH/NF was rinsed with ethanol and water, followed by air drying for 8 h.

3.4. Characterization of Fe-NiCo LDH NSs

The crystal structure of the samples was analyzed by using X-ray diffraction (XRD) obtained by XRD-7000 X-RAY DIFFRACTOMETER, SHIMADZU Corporation (Japan). The morphologies were characterized with scanning electron microscopy (SEM) and transmission electron microscopy (TEM) were taken using FE-SEM S-4700, Hitachi, and TEM, JEM-2100F, JEOL Ltd., Tokyo, Japan, respectively. The elemental composition and distribution were investigated with energy dispersive X-ray spectroscopy (EDS, JEOL-2010) attached to scanning electron microscopy (SEM, S-4700). X-ray photoelectron spectroscopy (XPS) was carried out to analyze the chemical composition, valence states of the constituent elements in the samples, characterization with K-α XPS (Thermo Scientific), Atomic force microscopy (AFM) was carried out to calculate the thickness, captured on a Park System (XE7, Seongnam, Korea), and electrochemical measurements were carried out by means of an Iviumstat electrochemical interface (Eindhoven, Netherlands).

3.5. Electrochemical Measurements

All electrochemical measurements were performed in a standard three-electrode system at Adama Science and Technology University, Applied Chemistry Department, using an Iviumstat (Eindhoven, Netherlands) workstation at room temperature while using the as-obtained catalysts on the NF as the working electrode (WE), Pt wire as the counter electrode (CE), and Ag/AgCl electrode as the reference electrode (RE) in 1M KOH as the electrolyte solution **(Figure S1)**. For the OER, the Linear Sweep Voltammograms (LSVs) were measured at the potential range from 0 to 1 V *versus* Ag/AgCl at a scan rate of 5 mV s^{-1}. Electrochemical impedance spectroscopy (EIS) was measured in a frequency range of 1×10^5 to 0.01 Hz at optimized potential of 1.5 V *versus* Ag/AgCl. Cyclic voltammograms (CVs) were tested from 0.3 - 0.4 V *versus* Ag/AgCl at different scan rates of 2, 4, 6, 8, and 10 mV s^{-1}, which are employed to estimate the double-layer capacitances (C_{dl}) of the catalysts. Chronoamperometry curves were obtained with a constant current density of 10 mA cm^{-2}. The potentials measured were converted to a reversible hydrogen electrode (RHE) as follows: (Gicha, Tufa, et al., 2021a)

$$E_{RHE} = E_{Ag/AgCl} + 0.059\,X\,pH + E_{Ag/AgCl}{}^{0} \quad (15)$$

The electrochemically active surface area (ECSA) was evaluated from the electrochemical double-layer capacitance (C_{dl}) by simple CV measurements in no apparent Faradaic region at different scan rates (Xie et al., 2017). It was estimated by the following equation:

$$\text{ECSA} = \frac{C_{DL}}{C_S} \quad (16)$$

where C_s is the specific capacitance.

Generally, the overpotential was estimated as follows:

$$\eta(V) = E_{RHE} - E_{eq} \quad (17)$$

where $\eta(V)$ is the overpotential, E_{RHE} is the applied potential, and E_{eq} is the equilibrium potential, which is the value equal to 1.23V.

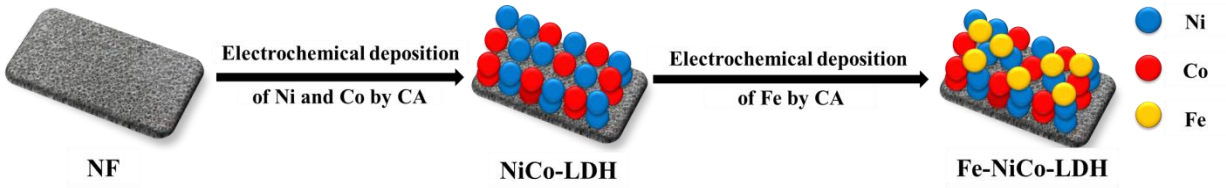

Scheme 1: Schematic illustration of the fabrication of Fe-NiCo LDH.

4. RESULTS AND DISCUSSION

4.1. Fabrication and Characterization of Fe-NiCo LDH NSs

The Fe-NiCo LDH NSs were prepared by a two-step electrochemical deposition method as illustrated in **Scheme 1**. First, NiCo LDH NSs were grown on the NF through a simple and cost effective electrochemical deposition method at an applied potential of −1.0 V *versus* Ag/AgCl for 300 s as previously reported elsewhere (Gicha, Tufa, et al., 2021b). NiCo LDH was cleaned with deionized (DI) water and left to dry, and then 2, 4, 6, and 8 mM of $FeSO_4.7H_2O$ solution was doped on NiCo LDH electrode by electrochemical deposition method at an applied potential of −1.0 V *versus* Ag/AgCl for 300 s. The electrochemical deposition process leads to the change of silvery NF to green color and then brown color, indicating successful deposition of the catalyst on the NF (**Figure S2**). **Figure S3** shows the cross-sectional SEM images of the Fe-NiCo LDH NSs with thickness of 688 nm. It is obvious that the Fe-NiCo LDH film has a layered NS structure, which are interconnected with each other to form a porous nanostructure.

The crystal structure of as-prepared Fe-NiCo LDH NSs were evaluated by XRD. As shown in Figure 2a, for a typical NiCo LDH and Fe-NiCo LDH samples, some of the peaks marked with vertical bars meet the standard plot of Ni double hydroxide (Ni DH) (JCPDS No. 00-038-0715) and Co double hydroxide (Co DH) (JCPDS No. 00-045-0031). Fe-NiCo/FTO (Fluorine doped tin oxide) film (JCPDS No. 01-077-0452) has been used instead of Fe-NiCo/NF film for XRD analysis due to the high background signal of Ni generated by NF. The diffraction peaks at 11.4^o, 24.0^o, 34.4^o, and 65.2^o can be assigned to the (003), (006), (012), and (110) facets of NiCo LDH hydrotalcite structure (Guo et al., 2020; T. Wang et al., 2017). In comparison, Fe-NiCo LDH has nearly identical XRD diffraction patterns with NiCo-LDH except the weaker peak intensity (peak broadening). This indicates that no new phase is formed, illustrating complete incorporation of Fe atoms into the NiCo DH lattice. The broadened reflections of the Fe-NiCo LDH product demonstrated the formation of small crystalline particles. The reflections show a slight shift to lower 2θ angle with Fe doping, revealing the lattice constants are shifted to higher values, implying substitutional incorporation of Fe ions into the NiCo DH structure (T. Wang et al., 2017). This result indicates the amorphous structure of Fe-NiCo LDH NSs. Therefore, based on the XRD results, the doping of Fe into the NiCo LDH system is successfully confirmed.

The high resolution TEM (HRTEM) was displayed in Figure 2b, where a lattice spacing distance (d) of 0.14 nm appeared, which agrees with the (110) of NiCo DH, demonstrating the formation of Fe-NiCo LDH. Surprisingly, the localized wavy lattice structure is also found in the HRTEM image of Fe-NiCo LDH (marked by the square box in Figures 2b), indicating the existence of planar defects, such as stacking faults, in some NSs, which might be induced by the Fe doping (Guo et al., 2020). In addition, some grain boundaries and edge sites were also observed (Figure 2b), suggesting the defective feature of the nanostructure (Yilmaz, Tan, Lim, & Ho, 2019). It is believed that such structure defects may cause exposure of more active sites and unsaturated sites for the electrocatalysis (Yilmaz et al., 2019).

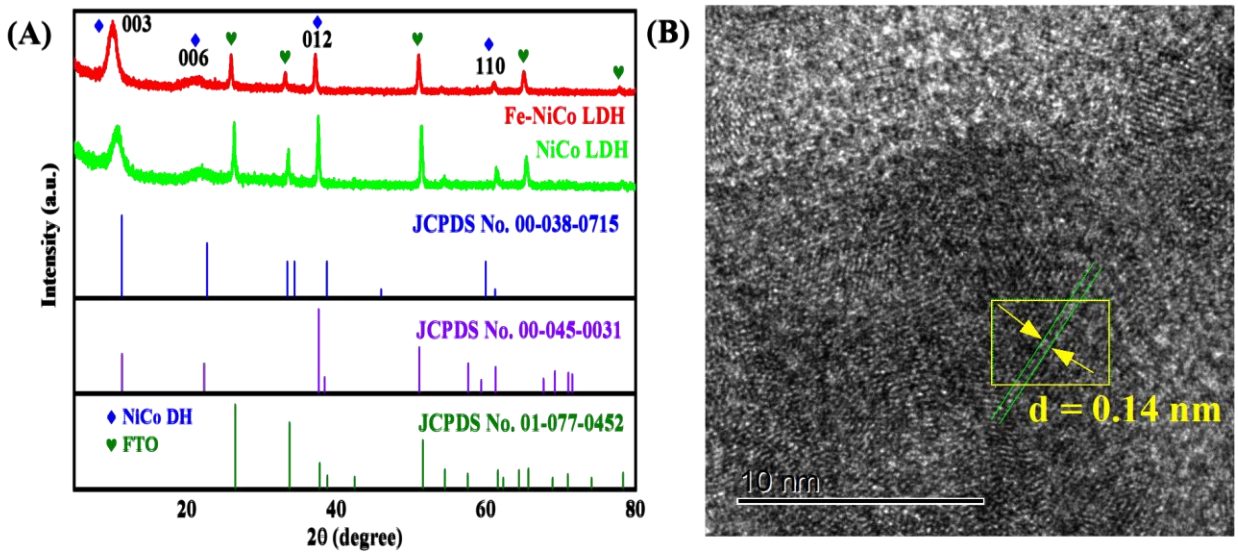

Figure 2: (a) XRD spectrum of bare FTO, NiCo LDH, and Fe-NiCo LDH material, (b) HRTEM of Fe-NiCo LDH.

The morphologies of the as-prepared samples were characterized by SEM. As shown in Figure 3a, all prepared samples displayed a hierarchical microstructure, with a nanosheet-assembled flower-like morphology. Furthermore, SEM images of Fe-NiCo LDH/NF at low magnification is shown in **Figure S4**. The NSs are interconnected with each other to form a porous nanostructure. The large pores in the coating layer contain many small pores to form a hierarchical 3D porous structure. SEM result demonstrates the successful preparation of 3D Fe-NiCo LDH NS on NF, which can expose rich active sites and provide fast ion diffusion pathways and efficient charge transferring conductive matrix during electrochemical reaction (L. Wan et al., 2021). To further study the detailed microstructure of the as-prepared products, the Fe-NiCo LDH were scratched

from the NF and examined by TEM. The TEM images of Fe-NiCo LDH show that all samples possess an interconnected, thin, and transparent sheet structure (Figure 3b). As illustrated in **Figure S5**, the TEM image of Fe-NiCo LDH were further indicated the nanosheet structure.

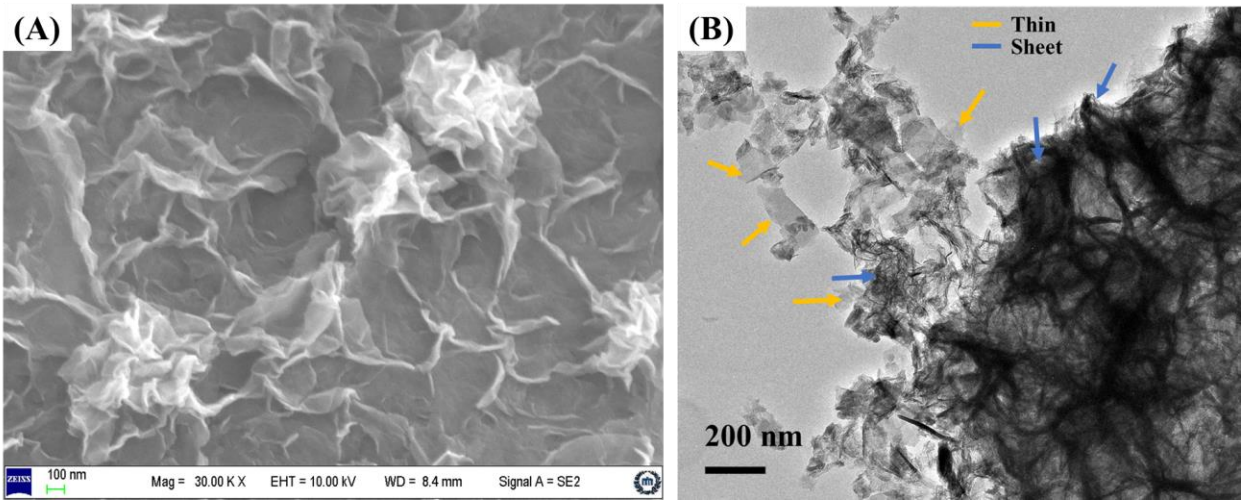

Figure 3: (a) SEM and (b) TEM image of Fe-NiCo LDH.

The 3D Fe-NiCo LDH-structured NS has a thickness of 7.2 nm as obtained from atomic force microscopy (AFM) for the optimized NiCo-4Fe sample (**Figure S6**). The ultrathin structure in Fe-NiCo LDH provides good conditions for the formation of the pore structure and shortens the distance to ion transfer. Thinner NSs are desired for OER because they can contain more active sites and the exposed surface atoms are easier to escape to form surface defects, thus enhancing the intrinsic activity of the LDH material (T. Wang et al., 2017).

Energy dispersive X-ray spectroscopy (EDS) elemental mapping (Figure 4) for the Fe-NiCo LDH/NF confirms homogeneous distribution of Ni, Co, Fe, and O elements throughout the sample, revealing that the Fe-NiCo LDH is successfully obtained. Figure 5 shows plots of SEM-EDS spectrum of Fe-NiCo LDH and verified the presence of Co, Ni, Fe and O. Table 2 illustrates the actual elemental composition in Fe-NiCo LDH sample determined by EDS analysis. Thus, the Fe-NiCo LDH sample exhibit a similar morphology and crystal structure (Figure 4).

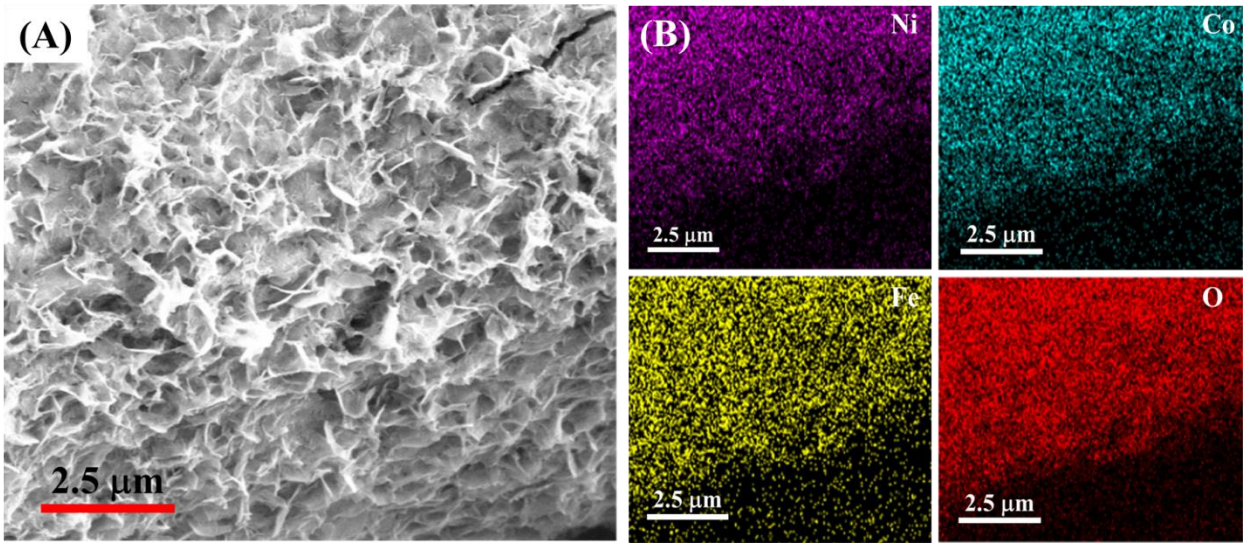

Figure 4: (a) SEM-EDS image, (b) The corresponding elemental mapping of Fe-NiCo LDH.

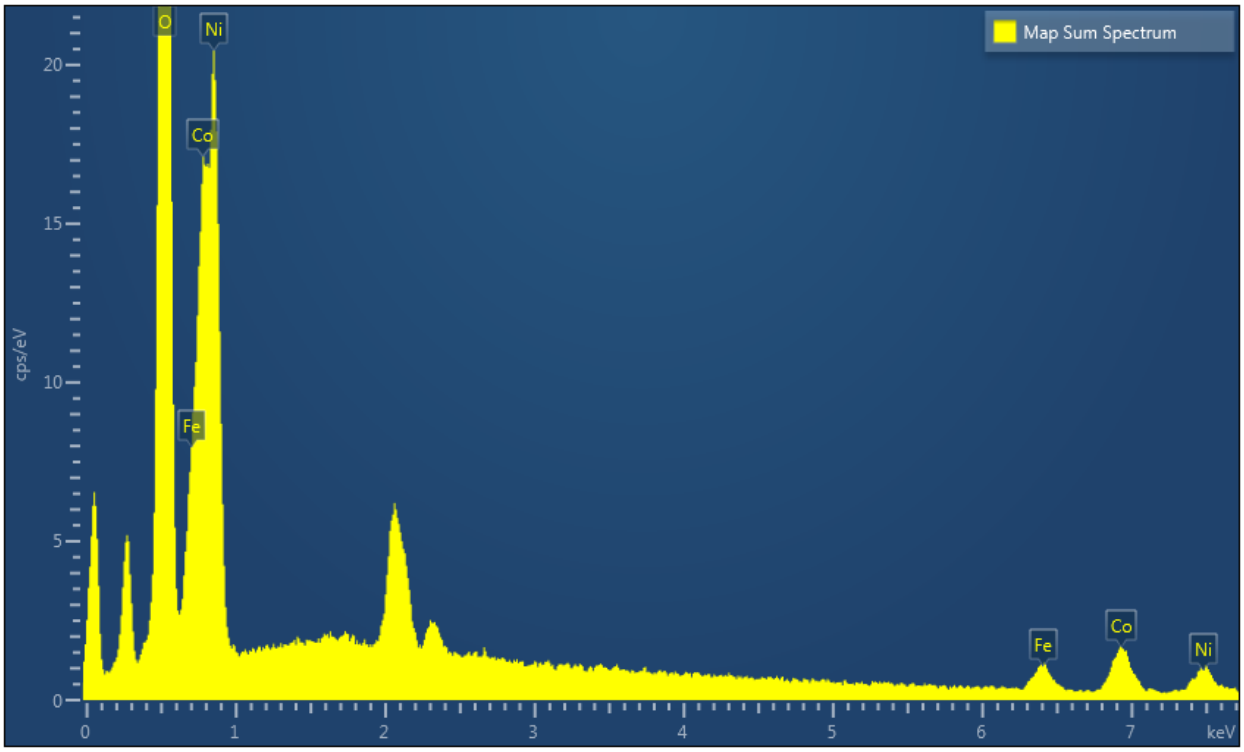

Figure 5: SEM-EDS spectrum of Fe-NiCo LDH.

Table 2: Elemental composition of Fe-NiCo LDH NSs sample from EDS analysis.

No.	Element	Atomic %
1	O	57.94
2	Fe	5.20
3	Co	16.99
4	Ni	19.87
Total		100.00

XPS analyses were then carried out to study the surface composition and chemical states of the as-prepared Fe-NiCo LDH/NF. The XPS survey spectrum of Fe-NiCo LDH/NF (Figure 6a) confirms the existence of Ni, Co, and Fe metals along with O. The high resolution XPS (HRXPS) spectra of Ni and Co are fitted to determine the chemical state of the cations. Two main peaks are found with the HRXPS spectrum of Ni 2p (Figure 7a) at 855.6 eV for Ni $2p_{3/2}$ and at 873.2 eV for Ni $2p_{1/2}$ orbits. Moreover, the spin-energy separation of 17.6 eV is characteristic of Ni^{2+}, which indicates the existence of $Ni(OH)_2$ on the surface (Ramachandran, Lan, Xu, & Wang, 2020; Septiani et al., 2020). The existence of different valence states of Co has also been confirmed by XPS. The two sharp peaks at 780.1 eV and 796.6 eV in the high-resolution XPS spectra of Co 2p can be indexed to Co $2p_{3/2}$ and Co $2p_{1/2}$, respectively (Figure 7b). The satellite peaks located at 785.5 and 802.5 eV are associated with the binding energy of Co^{2+}, and the low intense peak appeared at 790.7 eV attributes to Co^{3+}, which demonstrates the presence of both Co^{2+} and Co^{3+} ions in the sample (Guo et al., 2020). The spin-orbit separation of 16.5 eV in the Co 2p spectrum confirms the formation of the $Co(OH)_2$ phase. As for the Fe 2p spectrum (Figure 7c), the two peaks located at 711.6 and 724.8 eV can be attributed to Fe $2p_{3/2}$ and Fe $2p_{1/2}$ of Fe^{3+}, respectively (Guo et al., 2020). In addition, the energy separation between Fe $2p_{1/2}$ and $2p_{3/2}$ is 13.2 eV, indicating the existence of $Fe(OH)_3$. The high resolution XPS spectrum of the O1s (Figure 7d) shows a single peak ascribed to -OH groups, further confirming that Ni, Co and Fe are in the form of $Ni(OH)_2$, $Co(OH)_2$, and $Fe(OH)_3$, respectively (M. Li et al., 2019). As compared to undoped NiCo LDH (Figure 6b), Fe-NiCo LDH contains Ni, Co, Fe, and O elements (Figure 6a) whereas undoped NiCo LDH contains Ni, Co, and O elements. According to XPS analysis, Fe-NiCo LDH has broader peaks and higher proportion of lattice

oxygen than undoped NiCo LDH due to increases of oxygen vacancies (Figure 6). Therefore, the above results demonstrated that the Fe-NiCo LDH (NiCoFeOH) was successfully fabricated.

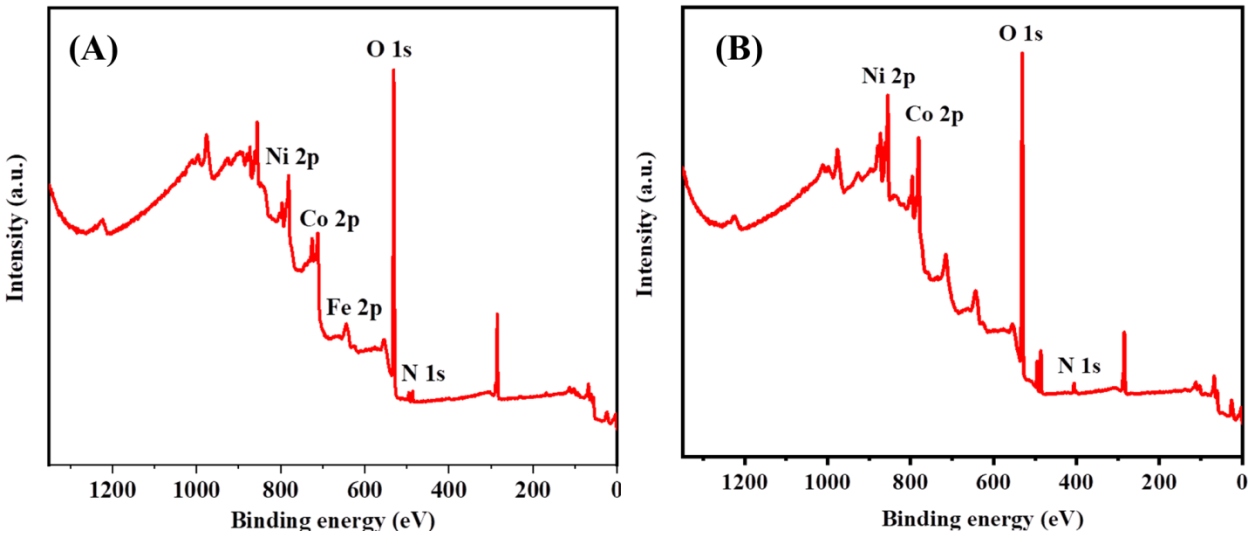

Figure 6: XPS survey plots of (a) Fe-doped NiCo LDH/NF and (b) Undoped NiCo LDH/NF.

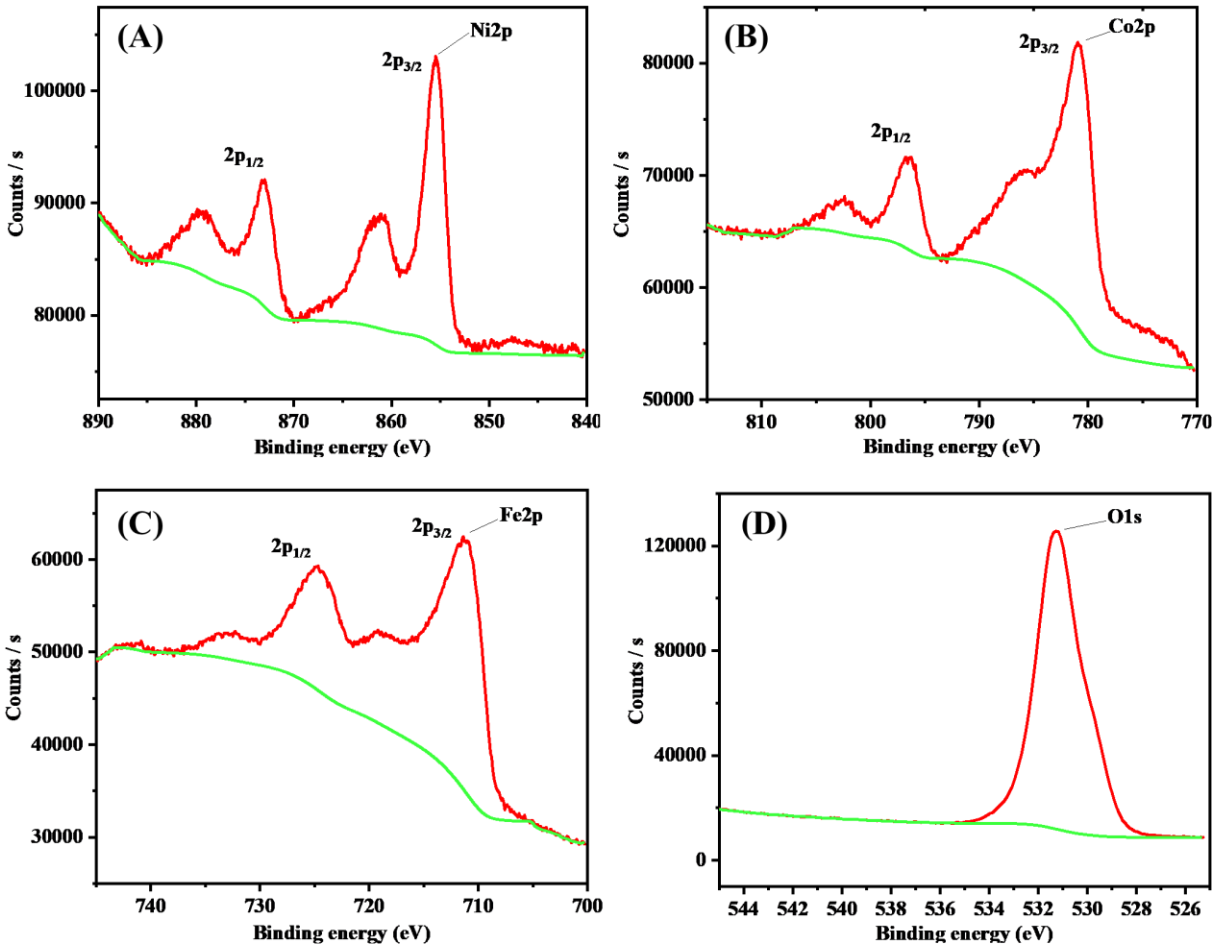

Figure 7: High-resolution XPS spectra of the Fe-NiCo LDH/NF: (a) Ni 2p, (b) Co 2p, (c) Fe 2p and (d) O 1s.

4.2. OER Catalytic Performance

The electrochemical performances of the as-fabricated electrodes were tested in a three-electrode configuration in a 1 M KOH aqueous electrolyte. Figure 8a compares the CV curves of bare NF, NiCo LDH, and different amounts of Fe-NiCo LDH/NF electrodes at a scan rate of 5 mV s^{-1}. A pair of weak redox peaks within the voltage of -0.3 – 0.5 V can be found for bare NF, suggesting its inferior kinetics for charge storage through surface redox reactions. Fe-doped and undoped NiCo LDH electrodes display a couple of noticeable redox peaks with obvious potential separation, which can be attributed to the reversible redox reactions of Ni^{2+}/Ni^{3+} and Co^{2+}/Co^{3+} (M. Li et al., 2019). Additionally, NiCo-4Fe/NF electrode exhibits the largest CV curve area among all electrodes, suggesting a highest specific capacity. Increasing dopant above 4Fe decreases the area of CV curve, due to over increasing of the size of NSs. By comparison, it can

be found that the integral area of the bare NF electrode is quite small, indicating that the contribution of NF to the total capacity of Fe-NiCo LDH/NF electrode is small. The CV curves (Figure 8b) indicate that the peak current of NiCo-4Fe/NF electrode increases without a significant change of the curve shape, and the peak potential shifts as the scan rate increases, which originates from the increased internal resistance under higher scan rates (L. Wan et al., 2021).

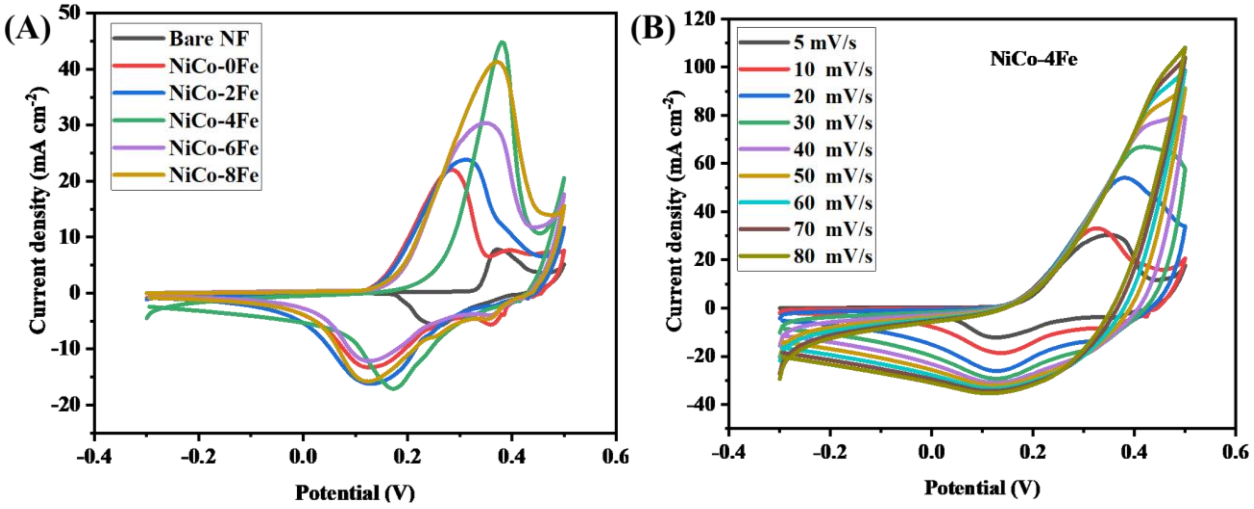

Figure 8: Electrochemical characteristics of the electrodes upon immersion in 1 M KOH aqueous solution. (a) CV curves recorded at a scan rate of 5 mV s^{-1}. (b) CV curves of NiCo-4Fe LDH at various scan rates.

To evaluate performance of the as-prepared Fe_x-NiCo LDH/NF, the electrocatalytic OER activity of the Fe_x-NiCo LDH/NF was investigated in 1.0 M KOH electrolyte using a standard three-electrode configuration. Figure 9a displays the LSV curves of various Fe-NiCo LDH catalysts with different amount of Fe doping. The observed peak between 0.2-0.4 V is attributed to the switch in oxidation state of Ni^{2+}/Co^{2+} to Ni^{3+}/Co^{3+}. Previously, Ni^{3+} was identified to be electrochemically more active than Ni^{2+}, whereas Co^{3+} was less active than Co^{2+}, however this change in oxidation state could improve the electrical conductivity, which in turn enhanced the overall OER activity of the catalyst (Guo et al., 2020; Septiani et al., 2020; H.-Y. Wang et al., 2016). The onset potential refers to the potential at which the catalyst can overcome all thermodynamic and kinetic barriers to produce a current. The potentials for NiCo-2Fe, NiCo-4Fe, NiCo-6Fe, and NiCo-8Fe are 0.496 V, 0.425 V, 0.467 V, and 0.485, respectively. Furthermore, the overpotentials required to generate a current density of 10 mA cm^{-2} (η_{10}) for

NiCo-2Fe, NiCo-4Fe, NiCo-6Fe, and NiCo-8Fe are 260 mV, 189 mV, 231 mV, and 249 mV, respectively (Figure 9b). In comparison, the potential for bare NF and NiCo-0Fe were 0.521 V, and 0.518 V, respectively. The overpotential for bare NF, and NiCo LDH/NF sample (NiCo-0Fe) are 285 mV, and 282 mV, respectively, which are greater than those of NiCo-2Fe, NiCo-4Fe, NiCo-6Fe, and NiCo-8Fe, indicating the benefit of Fe doping for enhancing the OER activity of NiCo-LDH (Figure 9b). The overpotential for bare NF is higher than that of NiCo-0Fe, which indicates NiCo-0Fe has higher catalytic activity than that of bare NF because NiCo-0Fe contains Ni and Co which increases the conductivity (Figure 9b).

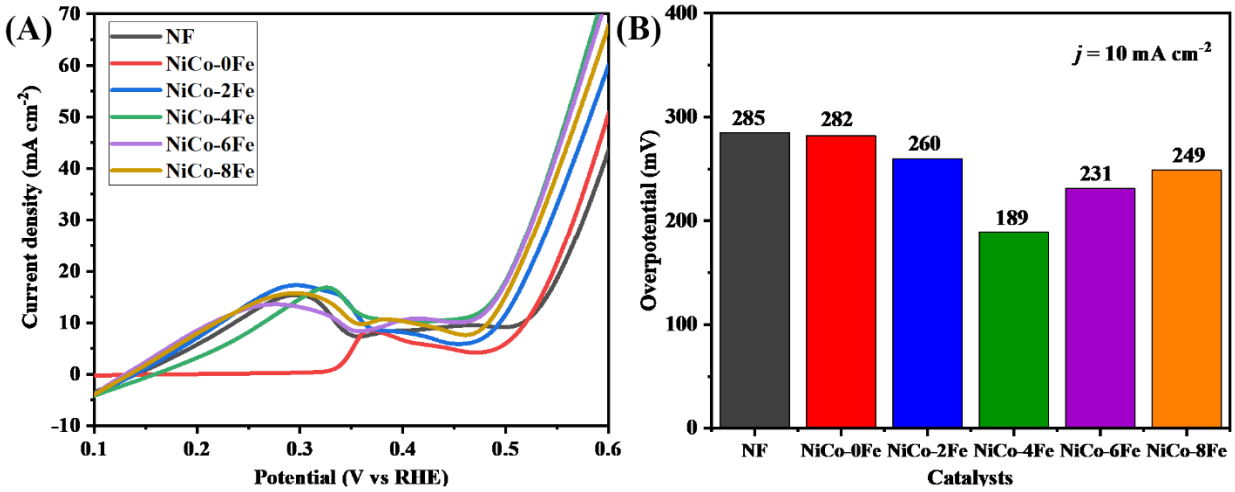

Figure 9: Electrochemical performance of various Fe-NiCo-LDH/NF electrodes carried out under a constant current density of 10 mA cm^{-2} in 1 M KOH aqueous solution. (a) OER polarization curves, (b) Overpotential comparison.

To investigate the OER kinetics of the as-prepared Fe-NiCo LDH catalysts, Tafel plots were derived from the LSV results. The Tafel plots reflect the relationship between the overpotential and the current density. As depicted in Figure 10, the Tafel slopes of NiCo-2Fe, NiCo-4Fe, NiCo-6Fe, and NiCo-8Fe are 124, 98.7, 116, and 121.8 mV dec^{-1}, respectively, whereas the Tafel slopes of the bare NF and NiCo-LDH sample (NiCo-0Fe) are 257 and 131.3 mV dec^{-1}, respectively (Figure 10). This solidifies the enhancing effect of the Fe doping on the OER activity of NiCo-LDH. Furthermore, the lower Tafel slope of NiCo-4Fe relative to the other samples reflects its superior electrocatalytic activity toward OER. Furthermore, the high electrocatalytic activity of NiCo-4Fe compares favorably with many previously reported LDH-based electrocatalysts, as shown in Table 3.

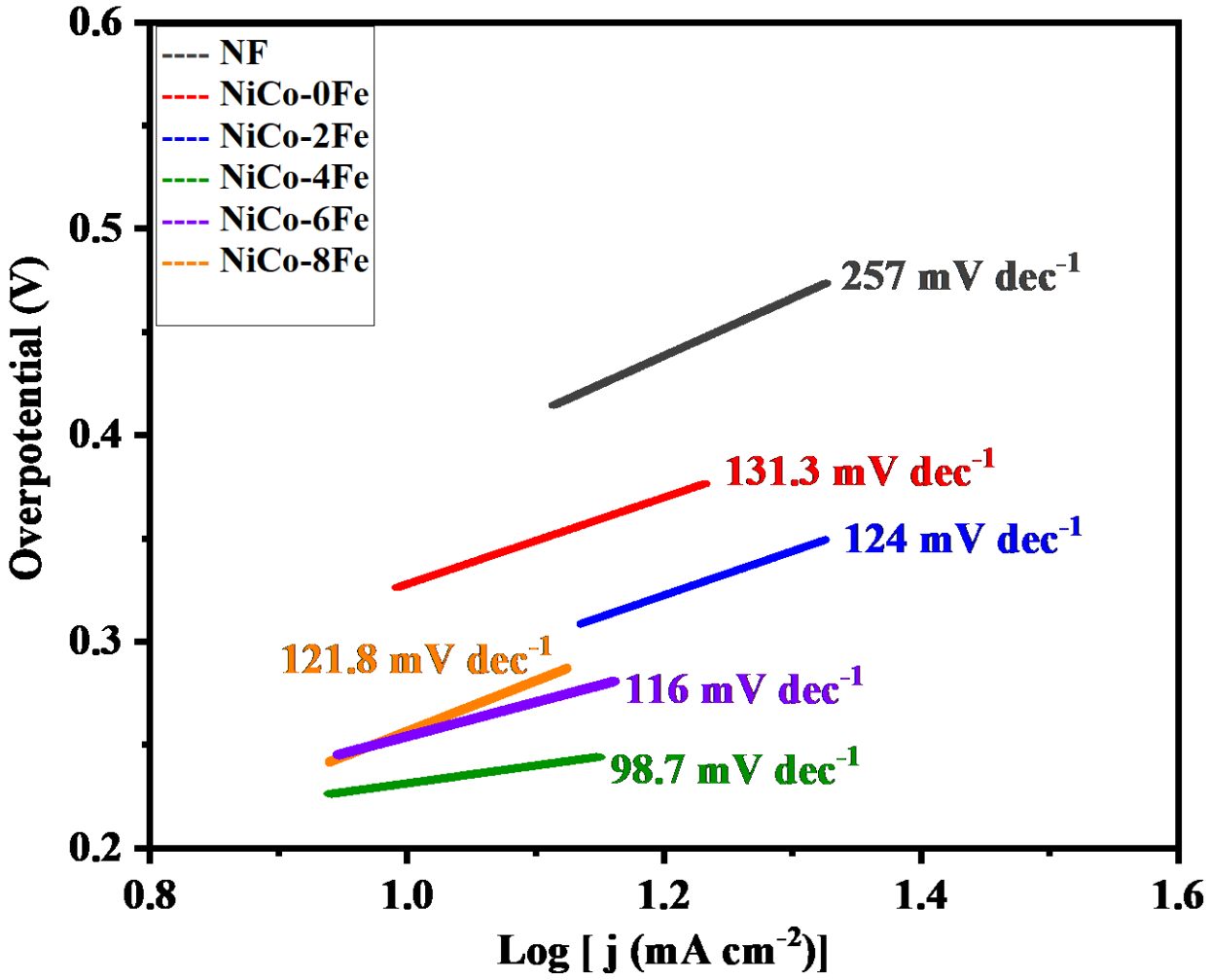

Figure 10: Tafel curve of various Fe-NiCo-LDH carried out under a constant current density of 10 mA cm^{-2}.

Table 3: Comparison of the electrocatalytic activity of the as-prepared Fe-NiCo LDH (current density of 10 mA cm^{-2}) NSs toward OER with previously reported LDH-based catalysts.

Catalyst	Electrolyte	Overpotential (η_{10}) (mV)	Tafel slope (mV dec^{-1})	Ref.
Fe-doped NiCo-LDH	**1 M KOH**	**189**	**98.7**	**This work**
CoFe LDHs	1 M KOH	300	83	(L. Feng et al., 2017)
Fe-doped NiCo-LDH	1 M KOH	285	62	(Septiani et al., 2020)

Ni-Co LDH	1 M KOH	291	45.6	(X. Ma et al., 2019)
Fe-Ni LDH	1 M KOH	261	85.5	(Zeng et al., 2018)
NiFe-LDH	0.1 M KOH	290	113	(Jiang, Zhang, Li, & Ai, 2015)
3D NiFe-LDH HMS	1M KOH	290	51	(Zhong et al., 2019)
NiGa-LDH	1M KOH	450	117	(Liang et al., 2015)
NiFe-LDH	1M KOH	310	76	(W. Ma et al., 2015)
ZnCo-LDH NS	1M KOH	385	108	(Qiu et al., 2020)

Note: Where η_{10} (overpotential at current density of 10 mA cm^{-2}), HMS (hollow microspheres), and NS (nanosheet).

To get further insights into OER performance of the as-prepared catalysts, the ECSA was estimated from C_{dl} in a non-faradaic potential range (0.3−0.4 V *vs.* Ag/AgCl) at various scan rates. The ECSA is an important parameter which determines the catalytic activity. A higher ECSA leads to an improvement in catalytic activity. In this work, the ECSAs of the Fe-NiCo LDH samples were investigated by checking the electrochemical C_{dl}. The CV measurements were conducted at various scan rates ranging from 2 to 10 mV s^{-1} in the potential window of 0.3−0.4 V *vs.* Ag/AgCl in 1 M KOH, as shown in Figure 11. NiCo-4Fe shows a C_{dl} of 1.44 mF cm^{-2}, noticeably larger than NiCo-2Fe (1.16 mF cm^{-2}), NiCo-6Fe (1.28 mF cm^{-2}), and NiCo-8Fe (1.18 mF cm^{-2}), indicating more exposed active sites with appropriate Fe doping and favorable for enhancing the OER activity of NiCo-4Fe (Figure 12). In addition, compared with bare NF (0.54 mF cm^{-2}) and NiCo-0Fe (1.12 mF cm^{-2}), all Fe_x-NiCo LDH samples possess larger C_{dl}, suggesting that Fe doping may generate more active sites in the electrode, which is possibly induced by the planar defects on the surface.

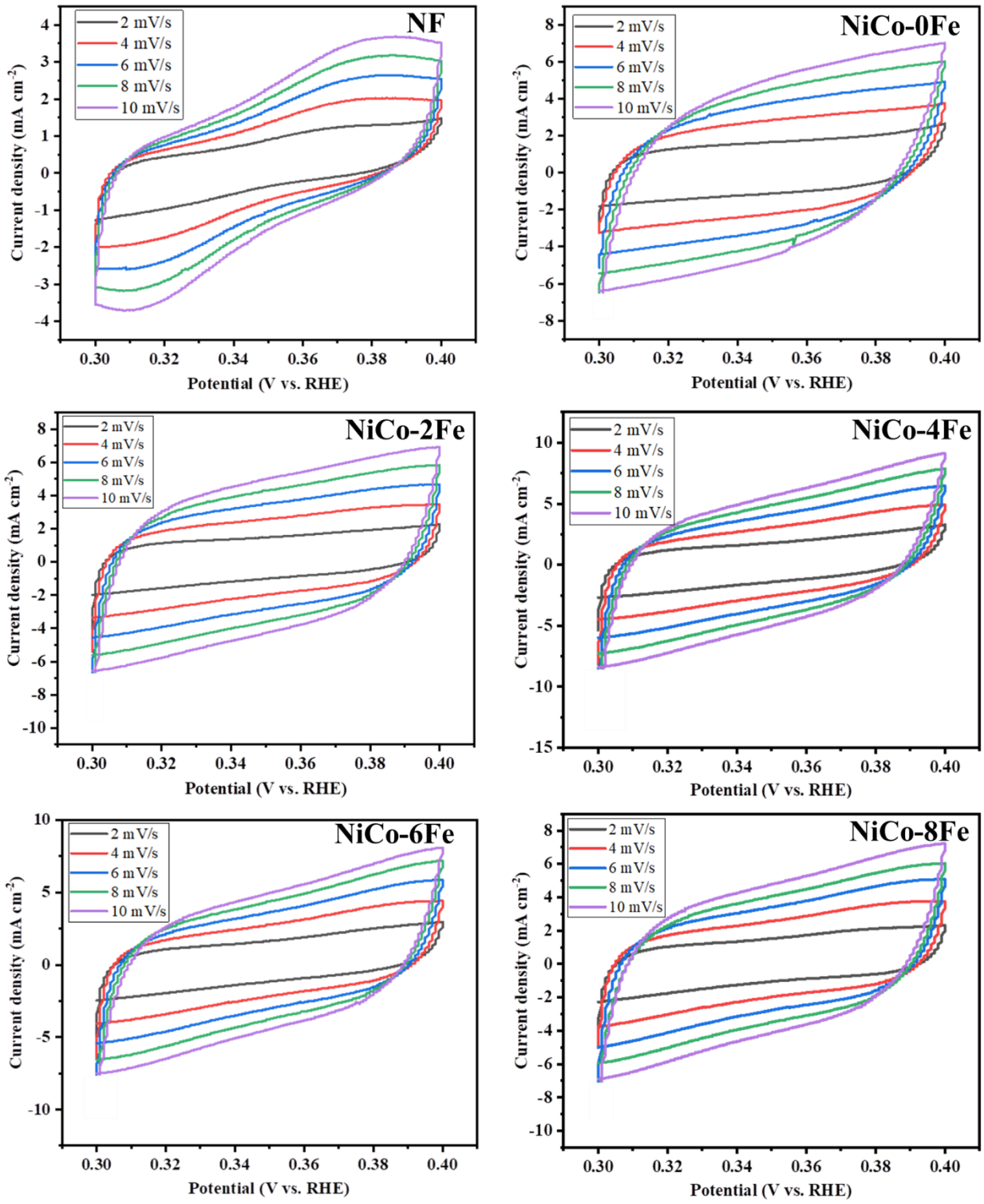

Figure 11: Double layer capacitance measurements with scan rates at 2, 4, 6, 8, and 10 mV/s in the region of 0.3–0.4 V *vs.* Ag/AgCl for Fe NiCo LDH/NF.

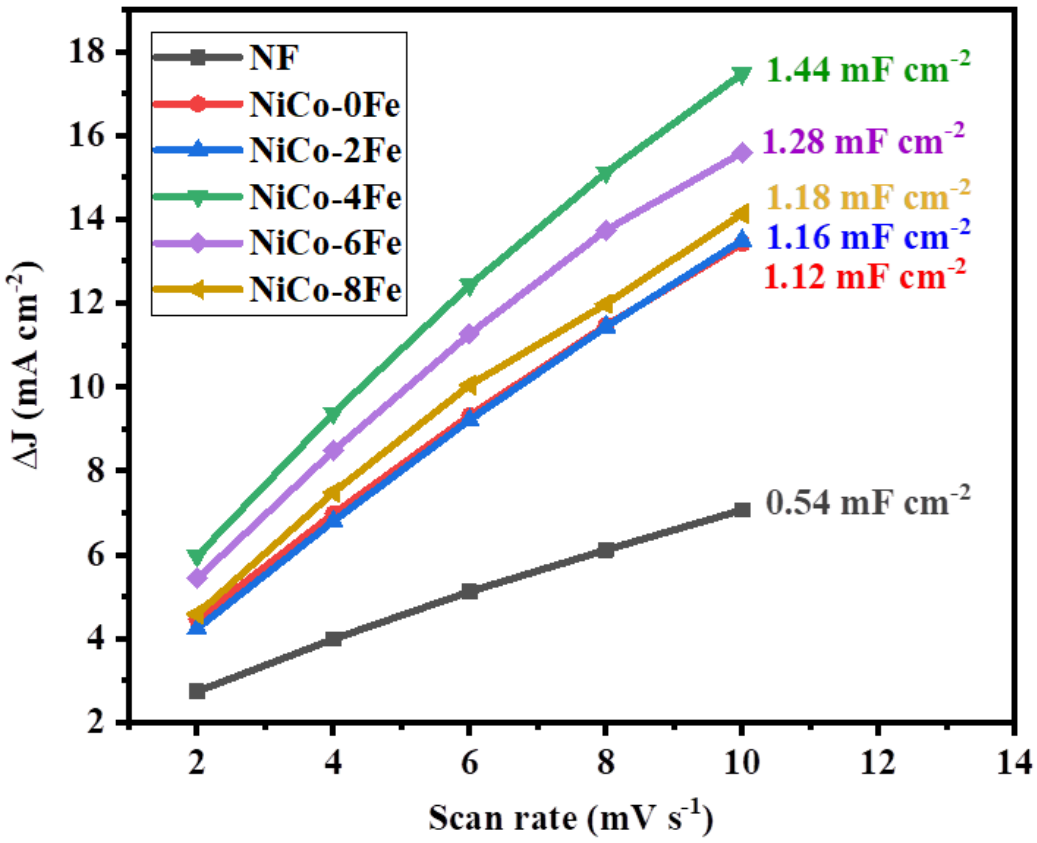

Figure 12: Capacitive current differences ($\Delta j = j_{anode} — j_{cathode}$) at 0.35 V vs RHE against scan rates of Fe-NiCo-LDH carried out under a constant current density of 10 mA cm^{-2}.

The C_{dl} can be further converted into ECSA using the specific capacitance value for a standard with 1cm^2 of real surface area. Specific capacitances have been measured for a variety of metal electrodes in acidic and alkaline solutions and typical values reported range between Cs = 0.015−0.110 mF cm^{-2} in H_2SO_4 and Cs = 0.022−0.130 mF cm^{-2} in NaOH and KOH solutions (Hou et al., 2016). The specific capacitance for a flat surface is normally between 0.02 - 0.06 mF cm^{-2}. For the purpose of this study, we use a specific capacitance of 0.04 mF cm^{-2}, which is a typical value for a metal electrode in aqueous 1M KOH solution based on typical reported values (Duan, Chen, Vasileff, & Qiao, 2016; Guo et al., 2020). The ECSA results, which have estimated from C_{dl} for different samples were summarized in (Table 4). Then, ECSA is calculated using the equation as follows:

$$ECSA = \frac{C_{dl}-catalyst(mF\ cm^{-2})}{0.04\ (mF\ cm^{-2})\ per\ ECSA\ cm^2} \quad (18)$$

Table 4: ECSA results estimated from C_{dl} for the as-fabricated samples for OER.

Catalysts	**C_{dl} (mF cm^{-2})**	**ECSA**
NF	0.54	13.5
NiCo-0Fe	1.12	28
NiCo-2Fe	1.16	29
NiCo-4Fe	1.44	36
NiCo-6Fe	1.28	32
NiCo-8Fe	1.18	29.5

In general, the OER activity of a catalyst is affected by several critical factors, such as ECSA and the electronic structure of the catalyst. The much higher surface area of NiCo-4Fe compared to those of other Fe-doped and undoped NiCo-LDH samples is beneficial for increasing the number of active sites which are involved in the oxidation reaction (Deng, Öztürk, Weidenthaler, & Tüysüz, 2017; Septiani et al., 2020). This leads to the higher OER activity of NiCo-4Fe relative to the other samples. This theory is supported by previous reports which noted a linear correlation between the specific surface area and OER activity of Co_3O_4 and $BiFeO_3$ systems, respectively (Papadas, Christodoulides, Kioseoglou, & Armatas, 2015; L. Xu et al., 2016). Another factor which affects the OER activity is the electronic structure of the catalyst. Generally, it is accepted that the metal-oxygen binding is a crucial factor which determines the OER activity due to the four-step catalytic reactions involving a series of intermediates, including M-OH, M-O, M-OOH, and M-OO, as expressed by the following equations: (C. Feng et al., 2020)

$$OH^- + * \rightarrow *OH + e^- \quad (19)$$

$$*OH + OH^- \rightarrow *O + H_2O + e^- \quad (20)$$

$$*O + OH^- \rightarrow *OOH + e^- \quad (21)$$

$$*OOH + OH^- \rightarrow * + O_2 + H_2O + e^- \quad (22)$$

where * denote the adsorption site of water molecules.

For a transition metal hydroxide, the occupancy of d states associated with the oxygen adsorption energy determines the OER activity (Gao & Yan, 2018). The higher the degree of overlap, the stronger the bonding. According to the density functional theory (DFT) study by Wang *et al*., Fe^{3+} could substitute Ni^{2+} and occupy Ni site in octahedral Ni (oxy) hydroxide structure. Such substitution is also likely due to the relatively close ionic radius of Fe^{3+} (60 ppm) relative to Ni^{2+} (70 ppm) and Co^{2+} (70 pm). The presence of Fe^{3+} can change the oxidation state of Ni or Co, which in turn can induce metal vacancies, distort the octahedron geometry, broaden d bands, and improve the orbital overlap with O-2p (Y. Wang et al., 2017). Consequently, the presence of metal vacancies can increase the valence state of nearby Ni and Co centers, decrease the coordination number of neighboring catalytic sites, and improve the adsorption of the OER intermediate, O* (Y. Wang, Qiao, Li, & Wang, 2018; Y. Wang et al., 2017). Further, the presence of Ni^{2+} and Co^{2+} can help to stabilize Fe^{3+} and connect Fe^{3+} to the conducting electrode (Zhong et al., 2017). The synergetic cooperation of all the above factors leads to the high electrocatalytic activity of NiCo-4Fe LDH. The sudden decrease in the OER activity of NiCo-8Fe may be attributed to the formation of electrically insulating FeOOH resulting from the high Fe content. This is reflected by the much higher charge transfer resistance of NiCo-8Fe compared to the rest of the Fe containing catalysts (Figure 13) (Burke, Enman, Batchellor, Zou, & Boettcher, 2015).

EIS measurement was further conducted to study electrode kinetics at the electrolyte/electrode interface. A Nyquist plot, having the real impedance component (Z′) on the x-axis, and the imaginary component (-Z″) on the y-axis, is fitted with equivalent electrical circuits to obtain the device properties in a quantitative way, as depicted in Figure 13 (Aguedo, Lorencova, Barath, Farkas, & Tkac, 2020). The charge transfer between the electrolyte and the electrocatalyst is another critical factor which influences the OER activity. The charge transfer resistance (R_{ct}) in low-frequency region can convey the electrocatalytic kinetics and a lower value corresponds to a faster rate of charge transfer. As shown in Figure 13, NiCo-4Fe has a small R_{ct} of 1.18 Ω, lower than bare NF (1.61 Ω) and NiCo-0Fe (1.54 Ω), suggesting a more rapid charge transfer rate that is beneficial for an efficient OER process. A smaller charge transfer resistance is realized on NiCo-4Fe compared to NiCo-2Fe, NiCo-6Fe, and NiCo-8Fe, suggesting a faster rate of charge

transfer in NiCo-4Fe for OER. The fundamental equivalent (Randel's) circuit illustrated in Figure 13 produces the Nyquist plot and the values of solution resistance (Rs) and R_{ct} are indicated. If the Nyquist plot has a semicircular shape with an intercept, the equivalent circuit consists of a constant phase element (CPE) in parallel with the R_{ct} or a CPE in parallel with the R_{ct} in series with Rs (Figure 13) (Merrill, 2007).

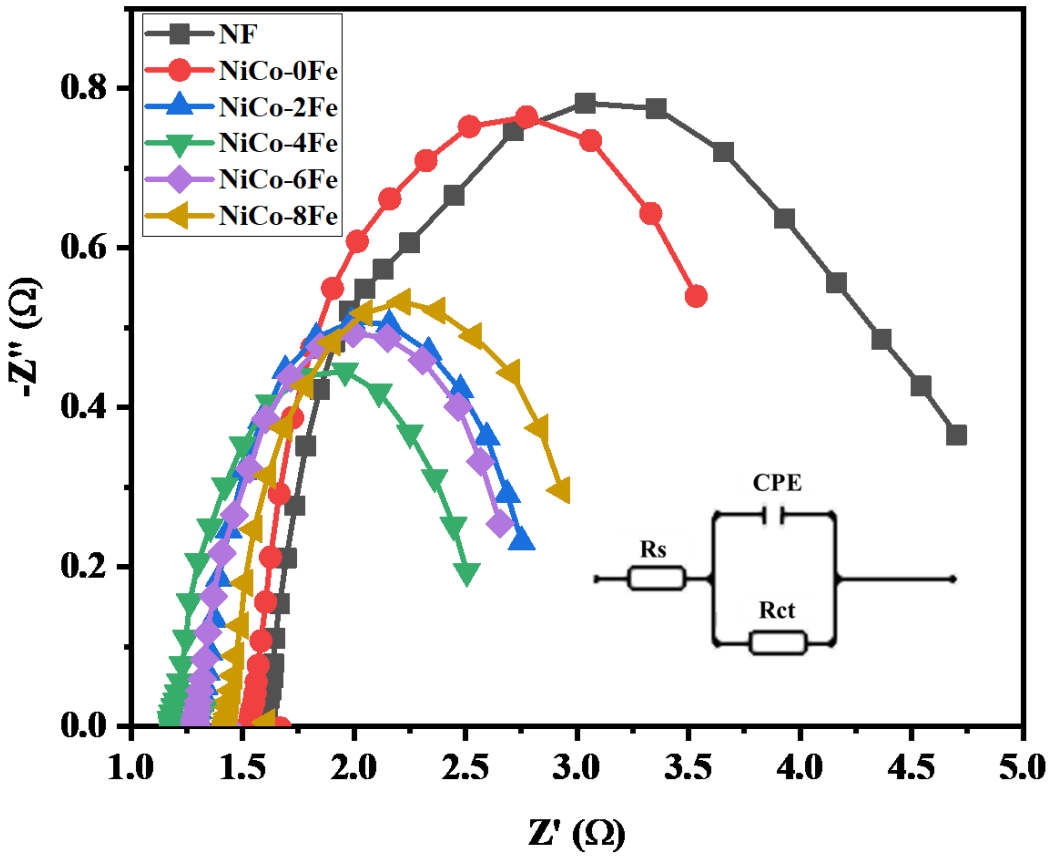

Figure 13: Nyquist plots of Fe-NiCo LDH carried out under a constant current density of 10 mA cm^{-2} and equivalent electrical circuit inset.

Chronoamperometric measurements were conducted for 12 h to test the stability of the optimum sample, NiCo-4Fe at current density of 10 mA cm^{-2}. As stability is an important factor for practical application of OER electrocatalysts, the best catalyst, NiCo-4Fe, is also assessed for durability. After continuous oxygen evolution in 1.0 M KOH at 10 mA cm^{-2} for 12 h, NiCo-4Fe shows negligible degradation in the overpotential (Figure 14a), indicating the remarkable long-term stability for the OER. Furthermore, the stability of the catalyst is tested using multistep chronopotentiometry as shown in Figure 14b. The current density increases from 5 to 40 mA

cm^{-2} with increments of 5 mA cm^{-2} per 500 s. With slight levels off potential at the beginning, it remained constant throughout the testing time, indicating the excellent mass transport, conductivity, and mechanical robustness of the electrode material (Guo et al., 2020).

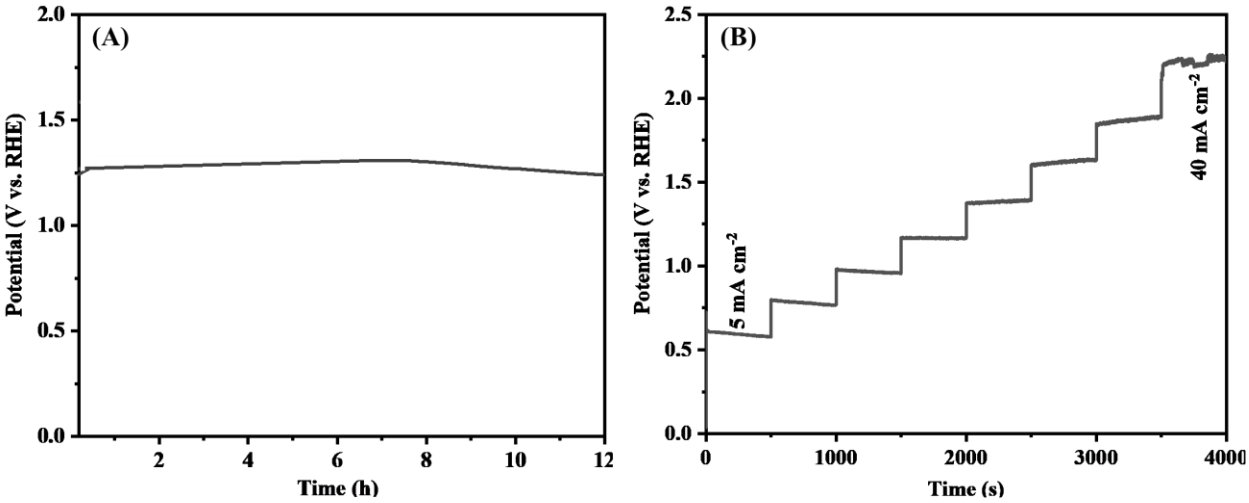

Figure 14: (a) Long-term stability test carried out under a constant current density of 10 mA cm^{-2}, (b) Multistep chronopotentiometric curve for Fe-NiCo LDH.

5. CONCLUSIONS AND RECOMMENDATIONS

5.1. Conclusions

In summary, the 3D Fe-NiCo LDH was synthesized through a typical electrochemical deposition process acted as catalyst of OER, displaying NS structure. The as-obtained Fe-NiCo LDH performs well as an effective electrocatalysts in 1.0 M KOH, which displays a superior catalytic activity to NiCo LDH toward OER. When utilized as an OER catalyst, the optimum Fe-NiCo LDH sample that showed a relatively low overpotential of 189 mV to produce a current density of 10 mA cm^{-2} and a low Tafel slope of 98.7 mV dec^{-1}. The good OER activity of the Fe-doped NiCo-LDH catalyst is attributed to several factors, including (i) the large specific surface area of the NSs which leads to enriched active sites for OER and (ii) improved ion transport and electrical conductivity induced by Fe doping and synergistic effects (as supported by the lower Tafel slope and charge transfer resistance compared to the undoped NiCo-LDH sample). Notably, Fe-NiCo LDH demonstrated good stability during the OER process, which is helpful for the long-term application. Thus, this work presents the importance of structural and compositional features of the electrocatalyst for high-performance OER, providing an efficient, cost effective, and competitive electrocatalyst for OER.

5.2. Recommendations

For the future study, there are a few recommendations on the computational simulations such as DFT to calculate adsorption free energies and mechanisms of Fe-NiCo LDH NSs that will give full information on active sites, which increases the catalytic activity. Furthermore, there are recommendations on the application of Fe-NiCo LDH for HER in order to compare the performance of it to OER and for supercapacitors.

Research Fund Acknowledgment

This research project is funded by Adama Science and Technology University under the grant number ASTU/SM-R/429/22, Adama, Ethiopia.

6. REFERENCES

Aguedo, J., Lorencova, L., Barath, M., Farkas, P., & Tkac, J. (2020). Electrochemical impedance spectroscopy on 2D nanomaterial MXene modified interfaces: application as a characterization and transducing tool. *Chemosensors*, *8*(4), 127.

Ahn, S. H., & Manthiram, A. (2020). Single Ni Atoms and Clusters Embedded in N-Doped Carbon "Tubes on Fibers" Matrix with Bifunctional Activity for Water Splitting at High Current Densities. *Small*, *16*(33), 2002511.

Anantharaj, S., Ede, S., Karthick, K., Sankar, S. S., Sangeetha, K., Karthik, P., & Kundu, S. (2018). Precision and correctness in the evaluation of electrocatalytic water splitting: revisiting activity parameters with a critical assessment. *Energy & Environmental Science*, *11*(4), 744-771.

Anantharaj, S., Ede, S. R., Sakthikumar, K., Karthick, K., Mishra, S., & Kundu, S. (2016). Recent trends and perspectives in electrochemical water splitting with an emphasis on sulfide, selenide, and phosphide catalysts of Fe, Co, and Ni: a review. *Acs Catalysis*, *6*(12), 8069-8097.

Anantharaj, S., Kundu, S., & Noda, S. (2021). "The Fe Effect": A review unveiling the critical roles of Fe in enhancing OER activity of Ni and Co based catalysts. *Nano Energy*, *80*, 105514.

Anantharaj, S., & Noda, S. (2020). Amorphous catalysts and electrochemical water splitting: an untold story of harmony. *Small*, *16*(2), 1905779.

Audichon, T., Napporn, T. W., Canaff, C., Morais, C. u., Comminges, C. m., & Kokoh, K. B. (2016). IrO2 coated on RuO2 as efficient and stable electroactive nanocatalysts for electrochemical water splitting. *The Journal of Physical Chemistry C*, *120*(5), 2562-2573.

Babar, P., Lokhande, A., Karade, V., Pawar, B., Gang, M. G., Pawar, S., & Kim, J. H. (2019). Bifunctional 2D electrocatalysts of transition metal hydroxide nanosheet arrays for water splitting and urea electrolysis. *ACS Sustainable Chemistry & Engineering*, *7*(11), 10035-10043.

Bhanja, P., Mohanty, B., Patra, A. K., Ghosh, S., Jena, B. K., & Bhaumik, A. (2019). IrO2 and Pt doped mesoporous SnO2 nanospheres as efficient electrocatalysts for the facile OER and HER. *ChemCatChem*, *11*(1), 583-592.

Burke, M. S., Enman, L. J., Batchellor, A. S., Zou, S., & Boettcher, S. W. (2015). Oxygen evolution reaction electrocatalysis on transition metal oxides and (oxy) hydroxides: activity trends and design principles. *Chemistry of Materials, 27*(22), 7549-7558.

Cai, C., Mi, Y., Han, S., Wang, Q., Liu, W., Wu, X., . . . Zhou, W. (2019). Engineering ordered dendrite-like nickel selenide as electrocatalyst. *Electrochimica Acta, 295*, 92-98.

Cai, Z., Bu, X., Wang, P., Ho, J. C., Yang, J., & Wang, X. (2019). Recent advances in layered double hydroxide electrocatalysts for the oxygen evolution reaction. *Journal of Materials Chemistry A, 7*(10), 5069-5089.

Cao, L.-M., Cao, Q.-C., Zhang, J., Zhu, X.-Y., Sun, R.-Z., Du, Z.-Y., & He, C.-T. (2021). Electrochemically Controlled Synthesis of Ultrathin Nickel Hydroxide Nanosheets for Electrocatalytic Oxygen Evolution. *Inorganic Chemistry, 60*(5), 3365-3374.

Cook, T. R., Dogutan, D. K., Reece, S. Y., Surendranath, Y., Teets, T. S., & Nocera, D. G. (2010). Solar energy supply and storage for the legacy and nonlegacy worlds. *Chemical reviews, 110*(11), 6474-6502.

Dai, L., Chen, Z. N., Li, L., Yin, P., Liu, Z., & Zhang, H. (2020). Ultrathin Ni (0)-embedded Ni (OH) 2 heterostructured nanosheets with enhanced electrochemical overall water splitting. *Advanced Materials, 32*(8), 1906915.

Darband, G. B., Aliofkhazraei, M., Hyun, S., Rouhaghdam, A. S., & Shanmugam, S. (2019). Electrodeposition of Ni–Co–Fe mixed sulfide ultrathin nanosheets on Ni nanocones: a low-cost, durable and high performance catalyst for electrochemical water splitting. *Nanoscale, 11*(35), 16621-16634.

Deng, X., Öztürk, S., Weidenthaler, C., & Tüysüz, H. (2017). Iron-induced activation of ordered mesoporous nickel cobalt oxide electrocatalyst for the oxygen evolution reaction. *ACS applied materials & interfaces, 9*(25), 21225-21233.

Dionigi, F., Zeng, Z., Sinev, I., Merzdorf, T., Deshpande, S., Lopez, M. B., . . . Fan, D. (2020). In-situ structure and catalytic mechanism of NiFe and CoFe layered double hydroxides during oxygen evolution. *Nature communications, 11*(1), 1-10.

Duan, J., Chen, S., Vasileff, A., & Qiao, S. Z. (2016). Anion and cation modulation in metal compounds for bifunctional overall water splitting. *ACS nano, 10*(9), 8738-8745.

Dutta, S., Indra, A., Feng, Y., Song, T., & Paik, U. (2017). Self-supported nickel iron layered double hydroxide-nickel selenide electrocatalyst for superior water splitting activity. *ACS applied materials & interfaces, 9*(39), 33766-33774.

Fan, H., Yu, H., Zhang, Y., Zheng, Y., Luo, Y., Dai, Z., . . . Yan, Q. (2017). Fe-doped Ni3C nanodots in N-doped carbon nanosheets for efficient hydrogen-evolution and oxygen-evolution electrocatalysis. *Angewandte Chemie International Edition, 56*(41), 12566-12570.

Feng, C., Faheem, M. B., Fu, J., Xiao, Y., Li, C., & Li, Y. (2020). Fe-based electrocatalysts for oxygen evolution reaction: progress and perspectives. *ACS Catalysis, 10*(7), 4019-4047.

Feng, L., Li, A., Li, Y., Liu, J., Wang, L., Huang, L., . . . Ge, X. (2017). A highly active CoFe layered double hydroxide for water splitting. *ChemPlusChem, 82*(3), 483-488.

Friebel, D., Louie, M. W., Bajdich, M., Sanwald, K. E., Cai, Y., Wise, A. M., . . . Alonso-Mori, R. (2015). Identification of highly active Fe sites in (Ni, Fe) OOH for electrocatalytic water splitting. *Journal of the American Chemical Society, 137*(3), 1305-1313.

Gao, R., & Yan, D. (2018). Fast formation of single-unit-cell-thick and defect-rich layered double hydroxide nanosheets with highly enhanced oxygen evolution reaction for water splitting. *Nano Research, 11*(4), 1883-1894.

Gicha, B. B., Tufa, L. T., Choi, Y., & Lee, J. (2021a). Amorphous Ni1–x Fe x Oxyhydroxide Nanosheets with Integrated Bulk and Surface Iron for a High and Stable Oxygen Evolution Reaction. *ACS Applied Energy Materials*.

Gicha, B. B., Tufa, L. T., Choi, Y., & Lee, J. (2021b). Amorphous Ni1–x Fe x Oxyhydroxide Nanosheets with Integrated Bulk and Surface Iron for a High and Stable Oxygen Evolution Reaction. *ACS Applied Energy Materials, 4*(7), 6833-6841.

Gicha, B. B., Tufa, L. T., Kang, S., Goddati, M., Bekele, E. T., & Lee, J. (2021). Transition metal-based 2D layered double hydroxide nanosheets: design strategies and applications in oxygen evolution reaction. *Nanomaterials, 11*(6), 1388.

Gong, M., Li, Y., Wang, H., Liang, Y., Wu, J. Z., Zhou, J., . . . Dai, H. (2013). An advanced Ni–Fe layered double hydroxide electrocatalyst for water oxidation. *Journal of the American Chemical Society, 135*(23), 8452-8455.

Görlin, M., Ferreira de Araújo, J., Schmies, H., Bernsmeier, D., Dresp, S. r., Gliech, M., . . . Dau, H. (2017). Tracking catalyst redox states and reaction dynamics in Ni–Fe oxyhydroxide

oxygen evolution reaction electrocatalysts: the role of catalyst support and electrolyte pH. *Journal of the American Chemical Society, 139*(5), 2070-2082.

Guo, M., Song, S., Zhang, S., Yan, Y., Zhan, K., Yang, J., & Zhao, B. (2020). Fe-doped Ni–Co phosphide nanoplates with planar defects as an efficient bifunctional electrocatalyst for overall water splitting. *ACS Sustainable Chemistry & Engineering, 8*(19), 7436-7444.

Hou, C.-C., Wang, C.-J., Chen, Q.-Q., Lv, X.-J., Fu, W.-F., & Chen, Y. (2016). Rapid synthesis of ultralong Fe (OH) 3: Cu (OH) 2 core–shell nanowires self-supported on copper foam as a highly efficient 3D electrode for water oxidation. *Chemical Communications, 52*(100), 14470-14473.

Hu, C., Wang, X., Yao, T., Gao, T., Han, J., Zhang, X., . . . Song, B. (2019). Enhanced Electrocatalytic Oxygen Evolution Activity by Tuning Both the Oxygen Vacancy and Orbital Occupancy of B-Site Metal Cation in NdNiO3. *Advanced Functional Materials, 29*(30), 1902449.

Huang, K., Dong, R., Wang, C., Li, W., Sun, H., & Geng, B. (2019). Fe–Ni layered double hydroxide arrays with homogeneous heterostructure as efficient electrocatalysts for overall water splitting. *ACS Sustainable Chemistry & Engineering, 7*(17), 15073-15079.

Hunter, B. M., Gray, H. B., & Muller, A. M. (2016). Earth-abundant heterogeneous water oxidation catalysts. *Chemical reviews, 116*(22), 14120-14136.

Jiang, J., Zhang, A., Li, L., & Ai, L. (2015). Nickel–cobalt layered double hydroxide nanosheets as high-performance electrocatalyst for oxygen evolution reaction. *Journal of Power Sources, 278*, 445-451.

Jing, C., Liu, X., Liu, X., Jiang, D., Dong, B., Dong, F., . . . Zhang, Y. (2018). Crystal morphology evolution of Ni–Co layered double hydroxide nanostructure towards high-performance biotemplate asymmetric supercapacitors. *CrystEngComm, 20*(46), 7428-7434.

Karmakar, A., Karthick, K., Sankar, S. S., Kumaravel, S., Madhu, R., & Kundu, S. (2021). A vast exploration of improvising synthetic strategies for enhancing the OER kinetics of LDH structures: a review. *Journal of Materials Chemistry A, 9*(3), 1314-1352.

Klaus, S., Cai, Y., Louie, M. W., Trotochaud, L., & Bell, A. T. (2015). Effects of Fe electrolyte impurities on Ni (OH) 2/NiOOH structure and oxygen evolution activity. *The Journal of Physical Chemistry C, 119*(13), 7243-7254.

Lasia, A. (2010). Hydrogen evolution reaction. *Handbook of fuel cells, 815*.

Li, L., Song, L., Guo, H., Xia, W., Jiang, C., Gao, B., . . . He, J. (2019). N-Doped porous carbon nanosheets decorated with graphitized carbon layer encapsulated Co 9 S 8 nanoparticles: An efficient bifunctional electrocatalyst for the OER and ORR. *Nanoscale, 11*(3), 901-907.

Li, M., Jijie, R., Barras, A., Roussel, P., Szunerits, S., & Boukherroub, R. (2019). NiFe layered double hydroxide electrodeposited on Ni foam coated with reduced graphene oxide for high-performance supercapacitors. *Electrochimica Acta, 302*, 1-9.

Li, N., Bediako, D. K., Hadt, R. G., Hayes, D., Kempa, T. J., Von Cube, F., . . . Nocera, D. G. (2017). Influence of iron doping on tetravalent nickel content in catalytic oxygen evolving films. *Proceedings of the National Academy of Sciences, 114*(7), 1486-1491.

Li, Y., Dong, Z., & Jiao, L. (2020). Multifunctional transition metal-based phosphides in energy-related electrocatalysis. *Advanced Energy Materials, 10*(11), 1902104.

Liang, H., Li, L., Meng, F., Dang, L., Zhuo, J., Forticaux, A., . . . Jin, S. (2015). Porous two-dimensional nanosheets converted from layered double hydroxides and their applications in electrocatalytic water splitting. *Chemistry of Materials, 27*(16), 5702-5711.

Liu, R., Wang, Y., Liu, D., Zou, Y., & Wang, S. (2017). Water-plasma-enabled exfoliation of ultrathin layered double hydroxide nanosheets with multivacancies for water oxidation. *Advanced Materials, 29*(30), 1701546.

Liu, W., Bao, J., Guan, M., Zhao, Y., Lian, J., Qiu, J., . . . Li, H. (2017). Nickel–cobalt-layered double hydroxide nanosheet arrays on Ni foam as a bifunctional electrocatalyst for overall water splitting. *Dalton Transactions, 46*(26), 8372-8376.

Liu, W., Cao, D., & Cheng, D. (2021). Review on synthesis and catalytic coupling mechanism of highly active electrocatalysts for water splitting. *Energy Technology, 9*(2), 2000855.

Liu, Y., Fu, N., Zhang, G., Xu, M., Lu, W., Zhou, L., & Huang, H. (2017). Design of Hierarchical Ni□ Co@ Ni□ Co Layered Double Hydroxide Core–Shell Structured Nanotube Array for High-Performance Flexible All-Solid-State Battery-Type Supercapacitors. *Advanced Functional Materials, 27*(8), 1605307.

Louie, M. W., & Bell, A. T. (2013). An investigation of thin-film Ni–Fe oxide catalysts for the electrochemical evolution of oxygen. *Journal of the American Chemical Society, 135*(33), 12329-12337.

Lu, X., Xue, H., Gong, H., Bai, M., Tang, D., Ma, R., & Sasaki, T. (2020). 2D layered double hydroxide nanosheets and their derivatives toward efficient oxygen evolution reaction. *Nano-Micro Letters*, *12*(1), 1-32.

Lu, Z., Qian, L., Tian, Y., Li, Y., Sun, X., & Duan, X. (2016). Ternary NiFeMn layered double hydroxides as highly-efficient oxygen evolution catalysts. *Chemical Communications*, *52*(5), 908-911.

Lv, L., Xu, K., Wang, C., Wan, H., Ruan, Y., Liu, J., . . . Lan, Y. (2016). Intercalation of glucose in NiMn-layered double hydroxide nanosheets: an effective path way towards battery-type electrodes with enhanced performance. *Electrochimica Acta*, *216*, 35-43.

Ma, R., Liu, Z., Takada, K., Iyi, N., Bando, Y., & Sasaki, T. (2007). Synthesis and exfoliation of Co2+− Fe3+ layered double hydroxides: an innovative topochemical approach. *Journal of the American Chemical Society*, *129*(16), 5257-5263.

Ma, W., Ma, R., Wang, C., Liang, J., Liu, X., Zhou, K., & Sasaki, T. (2015). A superlattice of alternately stacked Ni–Fe hydroxide nanosheets and graphene for efficient splitting of water. *ACS nano*, *9*(2), 1977-1984.

Ma, X., Wei, P., Yang, Y., Kang, H., Guo, D., & Liu, L. (2019). One-pot synthesis of Ni-Co layered double hydroxide nanosheets as efficient catalysts for oxygen evolution reaction. *Materials Today Communications*, *20*, 100596.

Martirez, J. M. P., & Carter, E. A. (2018). Unraveling oxygen evolution on iron-doped β-nickel oxyhydroxide: The key role of highly active molecular-like sites. *Journal of the American Chemical Society*, *141*(1), 693-705.

Merrill, M. D. (2007). *Water electrolysis at the thermodynamic limit*: The Florida State University.

Nai, J., Lu, Y., Yu, L., Wang, X., & Lou, X. W. (2017). Formation of Ni–Fe mixed diselenide nanocages as a superior oxygen evolution electrocatalyst. *Advanced Materials*, *29*(41), 1703870.

Papadas, I., Christodoulides, J. A., Kioseoglou, G., & Armatas, G. S. (2015). A high surface area ordered mesoporous BiFeO 3 semiconductor with efficient water oxidation activity. *Journal of Materials Chemistry A*, *3*(4), 1587-1593.

Qian, L., Lu, Z., Xu, T., Wu, X., Tian, Y., Li, Y., . . . Duan, X. (2015). Trinary layered double hydroxides as high-performance bifunctional materials for oxygen electrocatalysis. *Advanced Energy Materials, 5*(13), 1500245.

Qiu, C., Cai, F., Wang, Y., Liu, Y., Wang, Q., & Zhao, C. (2020). 2-Methylimidazole directed ambient synthesis of zinc-cobalt LDH nanosheets for efficient oxygen evolution reaction. *Journal of Colloid and Interface Science, 565*, 351-359.

Ramachandran, R., Lan, Y., Xu, Z.-X., & Wang, F. (2020). Construction of NiCo-layered double hydroxide microspheres from Ni-MOFs for high-performance asymmetric supercapacitors. *ACS Applied Energy Materials, 3*(7), 6633-6643.

Septiani, N. L. W., Kaneti, Y. V., Guo, Y., Yuliarto, B., Jiang, X., Ide, Y., . . . Sugahara, Y. (2020). Holey assembly of two-dimensional iron-doped nickel-cobalt layered double hydroxide nanosheets for energy conversion application. *ChemSusChem, 13*(6), 1645-1655.

Shakeel, M., Arif, M., Yasin, G., Li, B., & Khan, H. D. (2019). Layered by layered Ni-Mn-LDH/g-C3N4 nanohybrid for multi-purpose photo/electrocatalysis: morphology controlled strategy for effective charge carriers separation. *Applied Catalysis B: Environmental, 242*, 485-498.

Shin, H., Xiao, H., & Goddard III, W. A. (2018). In silico discovery of new dopants for Fe-doped Ni oxyhydroxide (Ni1–x Fe x OOH) catalysts for oxygen evolution reaction. *Journal of the American Chemical Society, 140*(22), 6745-6748.

Subbaraman, R., Tripkovic, D., Chang, K.-C., Strmcnik, D., Paulikas, A. P., Hirunsit, P., . . . Markovic, N. M. (2012). Trends in activity for the water electrolyser reactions on 3 d M (Ni, Co, Fe, Mn) hydr (oxy) oxide catalysts. *Nature materials, 11*(6), 550-557.

Sumboja, A., Chen, J., Zong, Y., Lee, P. S., & Liu, Z. (2017). NiMn layered double hydroxides as efficient electrocatalysts for the oxygen evolution reaction and their application in rechargeable Zn–air batteries. *Nanoscale, 9*(2), 774-780.

Sun, Z., Wang, Y., Lin, L., Yuan, M., Jiang, H., Long, R., . . . Sun, G. (2019). Engineering borate modified NiFe layer double hydroxide nanoarrays as “hydroxyl ions hungry” electrocatalysts for enhanced oxygen evolution. *Chemical Communications, 55*(9), 1334-1337.

Trotochaud, L., Ranney, J. K., Williams, K. N., & Boettcher, S. W. (2012). Solution-cast metal oxide thin film electrocatalysts for oxygen evolution. *Journal of the American Chemical Society, 134*(41), 17253-17261.

Tufa, L. T., Gicha, B. B., Wu, H., & Lee, J. (2021). Fe-Based Mesoporous Nanostructures for Electrochemical Conversion and Storage of Energy. *Batteries & Supercaps, 4*(3), 429-444.

Walter, C., Menezes, P. W., & Driess, M. (2021). Perspective on intermetallics towards efficient electrocatalytic water-splitting. *Chemical Science, 12*(25), 8603-8631.

Wan, L., Wang, Y., Zhang, Y., Du, C., Chen, J., Xie, M., . . . Zhang, W. (2021). Designing FeCoP@ NiCoP heterostructured nanosheets with superior electrochemical performance for hybrid supercapacitors. *Journal of Power Sources, 506*, 230096.

Wan, S., Qi, J., Zhang, W., Wang, W., Zhang, S., Liu, K., . . . Cao, R. (2017). Hierarchical Co (OH) F Superstructure Built by Low-Dimensional Substructures for Electrocatalytic Water Oxidation. *Advanced Materials, 29*(28), 1700286.

Wang, A.-L., Xu, H., & Li, G.-R. (2016). NiCoFe layered triple hydroxides with porous structures as high-performance electrocatalysts for overall water splitting. *ACS Energy Letters, 1*(2), 445-453.

Wang, H.-Y., Hung, S.-F., Chen, H.-Y., Chan, T.-S., Chen, H. M., & Liu, B. (2016). In operando identification of geometrical-site-dependent water oxidation activity of spinel Co3O4. *Journal of the American Chemical Society, 138*(1), 36-39.

Wang, J., Yue, X., Yang, Y., Sirisomboonchai, S., Wang, P., Ma, X., . . . Guan, G. (2020). Earth-abundant transition-metal-based bifunctional catalysts for overall electrochemical water splitting: A review. *Journal of Alloys and Compounds, 819*, 153346.

Wang, T., Xu, W., & Wang, H. (2017). Ternary NiCoFe layered double hydroxide nanosheets synthesized by cation exchange reaction for oxygen evolution reaction. *Electrochimica Acta, 257*, 118-127.

Wang, Y., Qiao, M., Li, Y., & Wang, S. (2018). Tuning surface electronic configuration of NiFe LDHs nanosheets by introducing cation vacancies (Fe or Ni) as highly efficient electrocatalysts for oxygen evolution reaction. *Small, 14*(17), 1800136.

Wang, Y., Zhang, Y., Liu, Z., Xie, C., Feng, S., Liu, D., . . . Wang, S. (2017). Layered double hydroxide nanosheets with multiple vacancies obtained by dry exfoliation as highly

efficient oxygen evolution electrocatalysts. *Angewandte Chemie International Edition, 56*(21), 5867-5871.

Wang, Z.-L., Xu, D., Xu, J.-J., & Zhang, X.-B. (2014). Oxygen electrocatalysts in metal–air batteries: from aqueous to nonaqueous electrolytes. *Chemical Society Reviews, 43*(22), 7746-7786.

Wang, Z., Liu, W., Hu, Y., Xu, L., Guan, M., Qiu, J., . . . Li, H. (2019). An Fe-doped NiV LDH ultrathin nanosheet as a highly efficient electrocatalyst for efficient water oxidation. *Inorganic Chemistry Frontiers, 6*(7), 1890-1896.

Wang, Z., Xu, S.-M., Xu, Y., Tan, L., Wang, X., Zhao, Y., . . . Song, Y.-F. (2019). Single Ru atoms with precise coordination on a monolayer layered double hydroxide for efficient electrooxidation catalysis. *Chemical Science, 10*(2), 378-384.

Wu, Z., Wang, X., Huang, J., & Gao, F. (2018). A Co-doped Ni–Fe mixed oxide mesoporous nanosheet array with low overpotential and high stability towards overall water splitting. *Journal of Materials Chemistry A, 6*(1), 167-178.

Wu, Z., Zou, Z., Huang, J., & Gao, F. (2018). Fe-doped NiO mesoporous nanosheets array for highly efficient overall water splitting. *Journal of catalysis, 358*, 243-252.

Xie, J., Zhang, X., Zhang, H., Zhang, J., Li, S., Wang, R., . . . Xie, Y. (2017). Intralayered Ostwald ripening to ultrathin nanomesh catalyst with robust oxygen-evolving performance. *Advanced Materials, 29*(10), 1604765.

Xu, H., Wang, B., Shan, C., Xi, P., Liu, W., & Tang, Y. (2018). Ce-doped NiFe-layered double hydroxide ultrathin nanosheets/nanocarbon hierarchical nanocomposite as an efficient oxygen evolution catalyst. *ACS applied materials & interfaces, 10*(7), 6336-6345.

Xu, L., Jiang, Q., Xiao, Z., Li, X., Huo, J., Wang, S., & Dai, L. (2016). Plasma-engraved Co3O4 nanosheets with oxygen vacancies and high surface area for the oxygen evolution reaction. *Angewandte Chemie, 128*(17), 5363-5367.

Yang, H., Wang, C., Zhang, Y., & Wang, Q. (2019). Green synthesis of NiFe LDH/Ni foam at room temperature for highly efficient electrocatalytic oxygen evolution reaction. *Science China Materials, 62*(5), 681-689.

Yang, L., Liu, Z., Zhu, S., Feng, L., & Xing, W. (2021). Ni-based layered double hydroxide catalysts for oxygen evolution reaction. *Materials Today Physics, 16*, 100292.

Yang, R., Zhou, Y., Xing, Y., Li, D., Jiang, D., Chen, M., . . . Yuan, S. (2019). Synergistic coupling of CoFe-LDH arrays with NiFe-LDH nanosheet for highly efficient overall water splitting in alkaline media. *Applied Catalysis B: Environmental, 253*, 131-139.

Ye, W., Fang, X., Chen, X., & Yan, D. (2018). A three-dimensional nickel–chromium layered double hydroxide micro/nanosheet array as an efficient and stable bifunctional electrocatalyst for overall water splitting. *Nanoscale, 10*(41), 19484-19491.

Yilmaz, G., Tan, C. F., Lim, Y. F., & Ho, G. W. (2019). Pseudomorphic transformation of interpenetrated prussian blue analogs into defective nickel iron selenides for enhanced electrochemical and photo-electrochemical water splitting. *Advanced Energy Materials, 9*(1), 1802983.

Yuan, C. Z., Sun, Z. T., Jiang, Y. F., Yang, Z. K., Jiang, N., Zhao, Z. W., . . . Xu, A. W. (2017). One-Step In Situ Growth of Iron–Nickel Sulfide Nanosheets on FeNi Alloy Foils: High-Performance and Self-Supported Electrodes for Water Oxidation. *Small, 13*(18), 1604161.

Zeng, L., Yang, L., Lu, J., Jia, J., Yu, J., Deng, Y., . . . Zhou, W. (2018). One-step synthesis of Fe-Ni hydroxide nanosheets derived from bimetallic foam for efficient electrocatalytic oxygen evolution and overall water splitting. *Chinese Chemical Letters, 29*(12), 1875-1878.

Zhang, H., Li, H., Akram, B., & Wang, X. (2019). Fabrication of NiFe layered double hydroxide with well-defined laminar superstructure as highly efficient oxygen evolution electrocatalysts. *Nano Research, 12*(6), 1327-1331.

Zhang, J., Liu, J., Xi, L., Yu, Y., Chen, N., Sun, S., . . . Zhang, B. (2018). Single-atom Au/NiFe layered double hydroxide electrocatalyst: probing the origin of activity for oxygen evolution reaction. *Journal of the American Chemical Society, 140*(11), 3876-3879.

Zhao, Q., Yang, J., Liu, M., Wang, R., Zhang, G., Wang, H., . . . Chen, H. (2018). Tuning electronic push/pull of Ni-based hydroxides to enhance hydrogen and oxygen evolution reactions for water splitting. *Acs Catalysis, 8*(6), 5621-5629.

Zhao, Z., Chen, C., Liu, Z., Huang, J., Wu, M., Liu, H., . . . Huang, Y. (2019). Pt-based nanocrystal for electrocatalytic oxygen reduction. *Advanced Materials, 31*(31), 1808115.

Zhong, H., Cheng, X., Xu, H., Li, L., Li, D., Tang, P., . . . Feng, Y. (2017). Carbon fiber paper supported interlayer space enlarged Ni2Fe-LDHs improved OER electrocatalytic activity. *Electrochimica Acta, 258*, 554-560.

Zhong, H., Liu, T., Zhang, S., Li, D., Tang, P., Alonso-Vante, N., & Feng, Y. (2019). Template-free synthesis of three-dimensional NiFe-LDH hollow microsphere with enhanced OER performance in alkaline media. *Journal of energy chemistry, 33*, 130-137.

Zhou, P., Wang, Y., Xie, C., Chen, C., Liu, H., Chen, R., . . . Wang, S. (2017). Acid-etched layered double hydroxides with rich defects for enhancing the oxygen evolution reaction. *Chemical Communications, 53*(86), 11778-11781.

Zou, X., & Zhang, Y. (2015). Noble metal-free hydrogen evolution catalysts for water splitting. *Chemical Society Reviews, 44*(15), 5148-5180.

Appendix

I. List of Publications/Manuscript in Preparation

1. **Molla, C.F**., Gonfa, B.A., Sabir, F.K., Gicha, B.B., Tufa, L.T.,*, J. Lee*. Ni-Based Ultrathin Nanostructures for Overall Electrochemical Water Splitting, submission preparation.

2. **Molla, C.F.**, Gonfa, B.A., Sabir, F.K., Gicha, B.B., Goddati, M., Feyie, E.K., Tufa, L.T.,* J. Lee*. Fe Modulation in NiCo Hydroxide Nanosheets for Efficient Oxygen Evolution Reaction, submission preparation.

3. Feyie, E.K., **Molla, C.F**., Tadesse, A.,*, Tufa, L.T.,*, Zereffa, E.A.*, J. Lee*. Novel Cu_4SnS_4/rGO composite electrode for high performance supercapacitors, manuscript in preparation.

II. Supporting Information

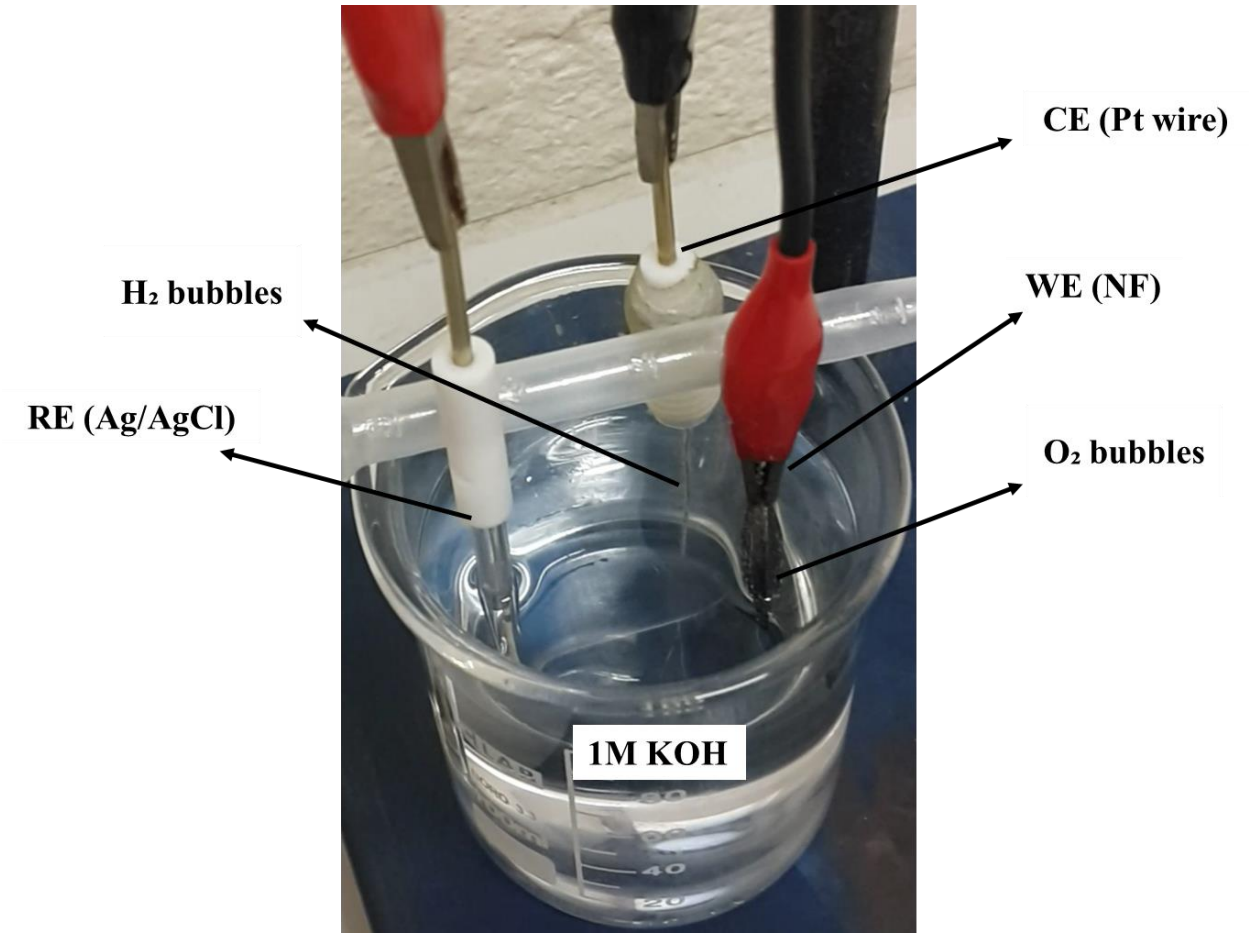

Figure S1. Digital photograph of three electrode system in which the Fe-NiCoOOH NSs was used as working electrode for electrocatalytic water splitting.

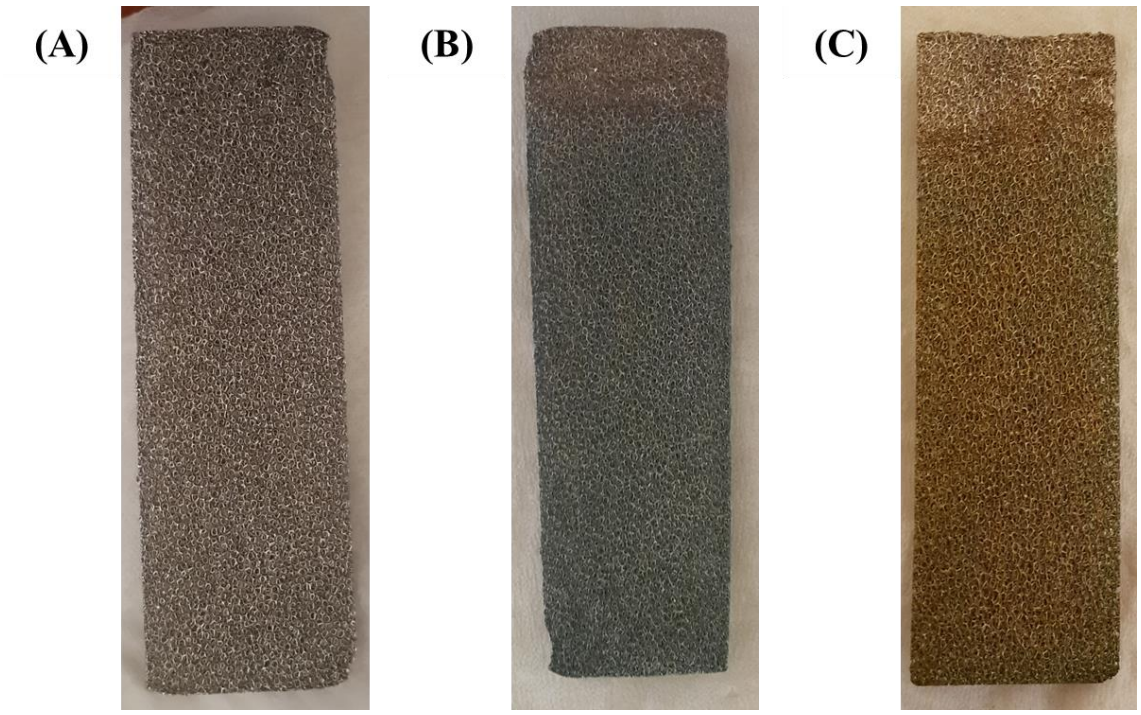

Figure S2. Digital photographs of (a) bare NF, (b) NiCo-LDH, and (c) Fe-NiCo-LDH.

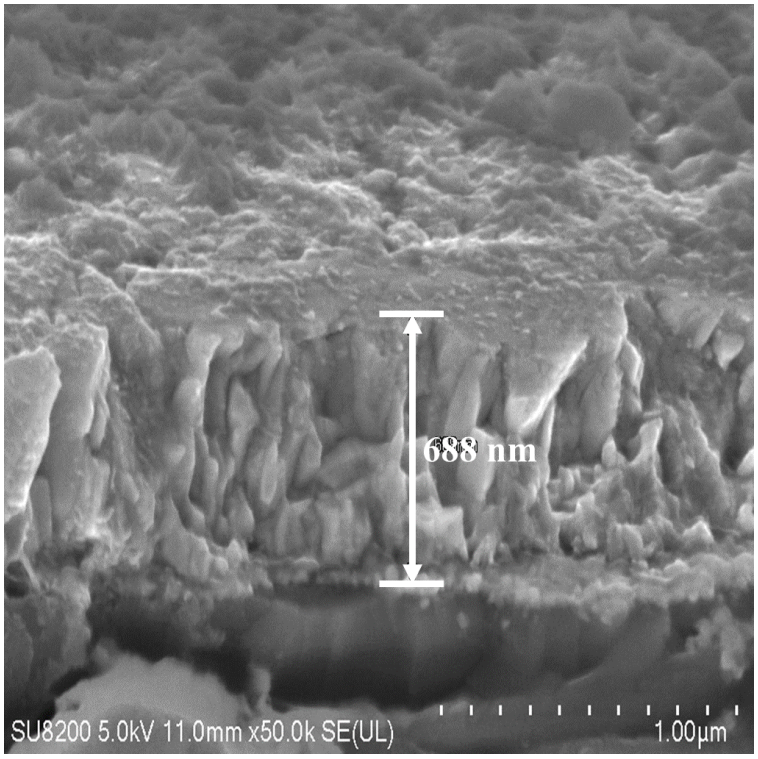

Figure S3. SEM cross-sectional image showing the thickness of the synthesized Fe-NiCo-LDH NSs.

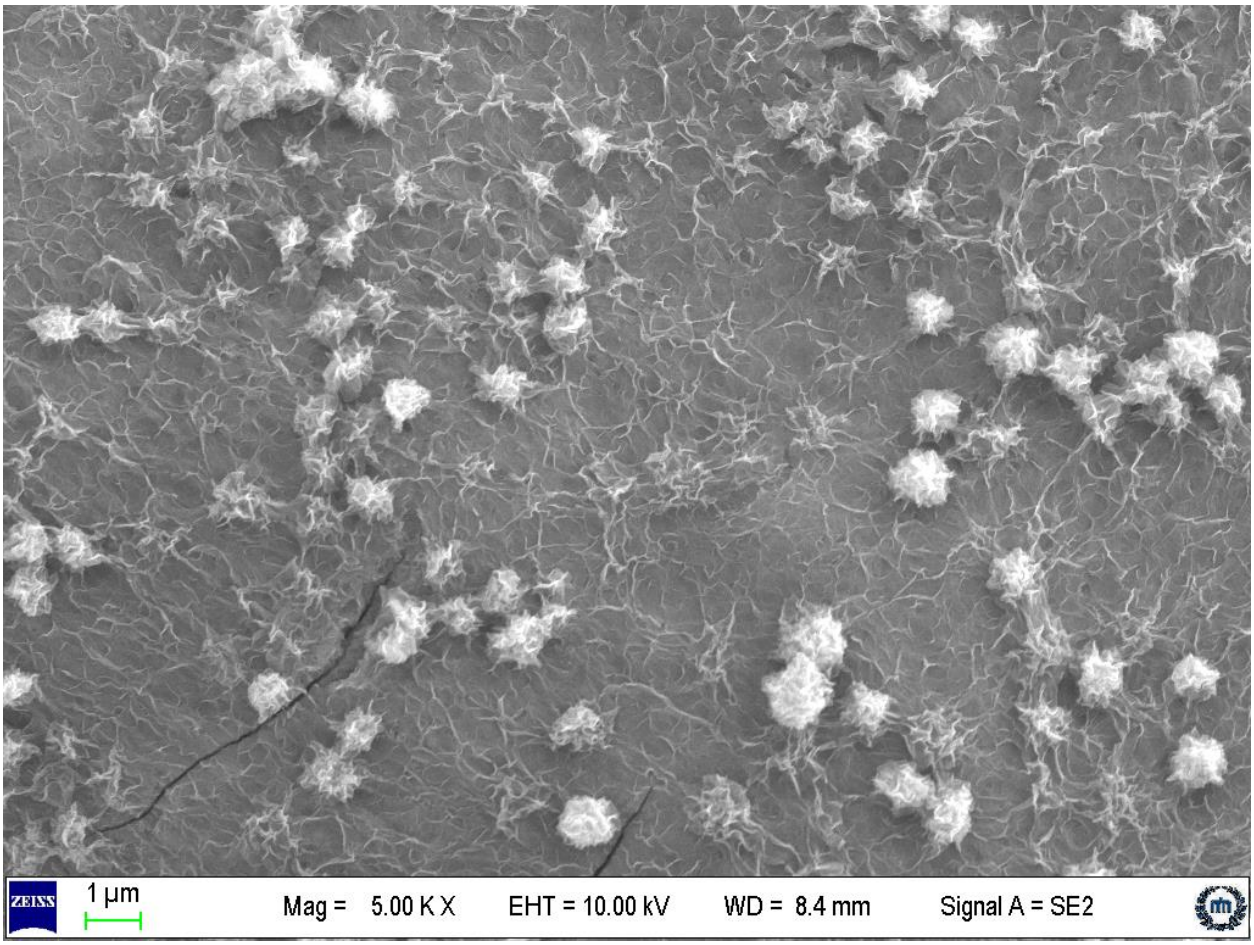

Figure S4: SEM images of low magnification of Fe-NiCo LDH.

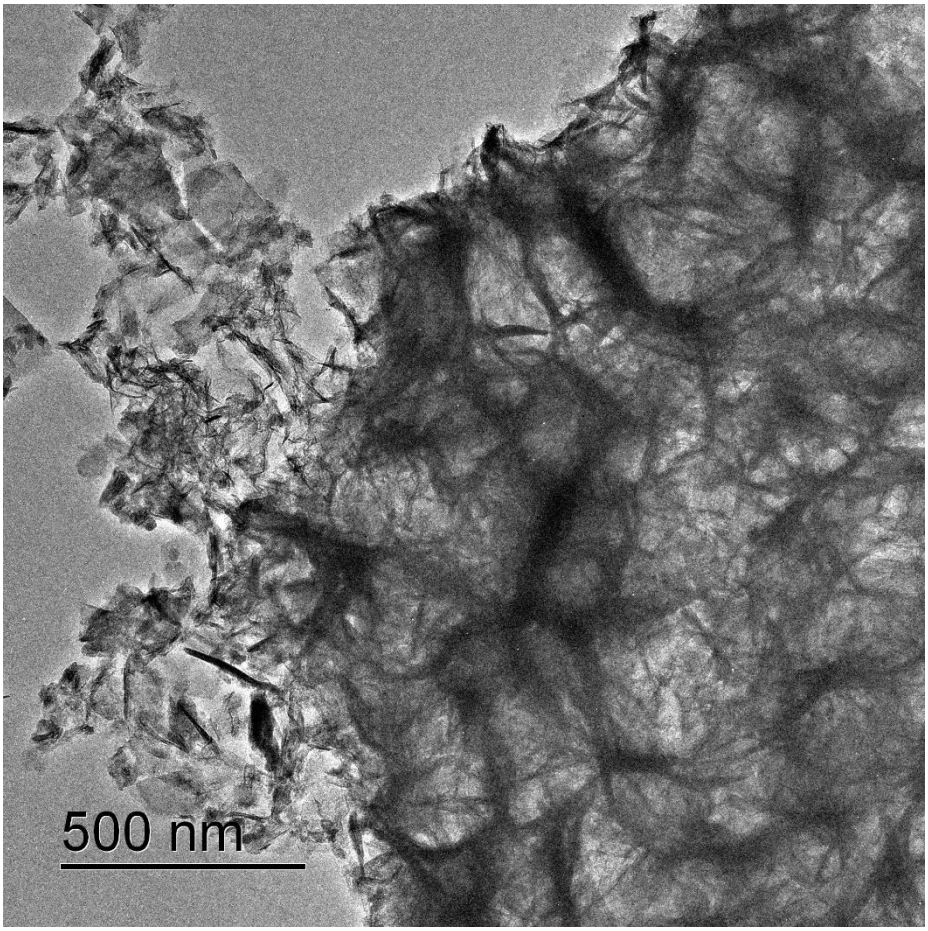

Figure S5: TEM images of Fe-NiCo LDH.

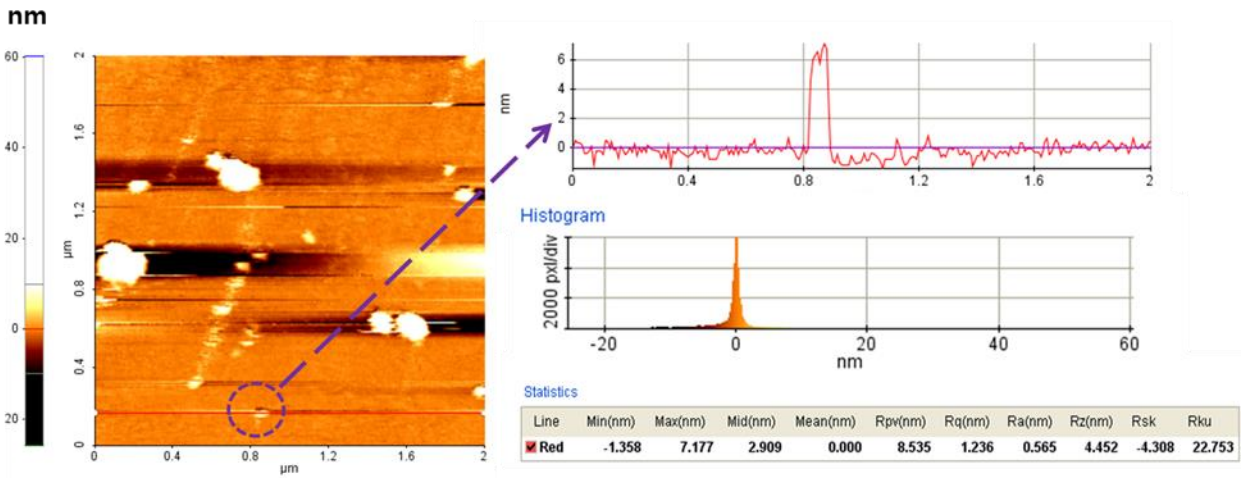

Figure S6: AFM image and corresponding height profile of Fe-NiCo LDH.